4. de Groot NG, Otting N, Doxiadis GG, et al. Evidence for an ancient selective sweep in the MHC class I gene repertoire of chimpanzees. Proc Natl Acad Sci USA 2002;99:11748-53.
5 Bontrop RE, Watkins DI. MHC polymorphism: AIDS susceptibility in non-human primates. Trends Immunol 2005;26:227-33.
6. Neel JV. Diabetes mellitus: A "thrifty" genotype rendered detrimental by "progress"? Am J Hum Genet 1962;14:353-62.
7. Nakajima T, Wooding S, Sakagami T, et al. Natural selection and population history in the human angiotensinogen gene (AGT): 736 complete AGT sequences in chromosomes from around the world. Am J Hum Genet 2004; 74:898-916.
8. Inoue I, Nakajima T, Williams CS, et al. A nucleotide substitution in the promoter of human angiotensinogen is associated with essential hypertension and affects basal transcription in vitro. J Clin Invest 1997;99:1786-97.
9. Hughes AL, Nei M. Pattern of nucleotide substitution at major histocompatibility complex class I loci reveals overdominant selection. Nature 1988;335: 167-70.
10. Horton R, Wilming L, Rand V, et al. Gene map of the extended human MHC. Nat Rev Genet 2004;5:889-99.
11. Pennacchio LA, Rubin EM. Genomic strategies to identify mammalian regulatory sequences. Nat Rev Genet 2001;2:100-9.
12. Ureta-Vidal A, Ettwiller L, Birney E. Comparative genomics: Genome-wide analysis in metazoan eukaryotes. Nat Rev Genet 2003;4:251-62.
13. Boffelli D, Nobrega MA, Rubin EM. Comparative genomics at the vertebrate extremes. Nat Rev Genet 2004;5:456-65.
14. Li WH. Molecular Evolution. Sinauer Associates, Inc 1997.
15. Miyata T, Yasunaga T. Molecular evolution of mRNA: A method for estimating evolutionary rates of synonymous and amino acid substitutions from homologous nucleotide sequences and its application. J Mol Evol 1980;16:23-36.
16. Nei M, Gojobori T. Simple methods for estimating the numbers of synonymous and nonsynonymous nucleotide substitutions. Mol Biol Evol 1986;3:418-26.
17. Li WH, Wu CI, Luo CC. A new method for estimating synonymous and nonsynonymous rates of nucleotide substitution considering the relative likelihood of nucleotide and codon changes. Mol Biol Evol 1985;2:150-74.
18. Yang Z. PAML 4: Phylogenetic analysis by maximum likelihood. Mol Biol Evol 2007;24:1586-91.
19. Chimpanzee Sequencing and Analysis Consortium. Initial sequence of the chimpanzee genome and comparison with the human genome. Nature 2005; 437:69-87.
20. Rhesus Macaque Genome Sequencing and Analysis Consortium, Gibbs RA, Rogers J, Katze MG, et al. Evolutionary and biomedical insights from the rhesus macaque genome. Science 2007;316:222-34.
21. Olson MV, Varki A. Sequencing the chimpanzee genome: Insights into human evolution and disease. Nat Rev Genet 2003;4:20-8.
22. Nielsen R, Bustamante C, Clark AG, et al. A scan for positively selected genes in the genomes of humans and chimpanzees. PLoS Biol 2005;3:e170.
23. Akira S, Uematsu S, Takeuchi O. Pathogen recognition and innate immunity. Cell 2006: 124: 783-801.

24. Bowie A, O'Neill LA. The interleukin-1 receptor/Toll-like receptor superfamily: Signal generators for pro-inflammatory interleukins and microbial products. J Leukoc Biol 2000;67:508-14.
25. Nakajima T, Ohtani H, Satta Y, et al. Natural selection in the TLR-related genes in the course of primate evolution. Immunogenetics 2008;60:727-35.
26. Poltorak A, He X, Smirnova I, et al. Defective LPS signaling in C3H/HeJ and C57BL/10ScCr mice: Mutations in Tlr4 gene. Science 1998;282:2085-8.
27. Shimazu R, Akashi S, Ogata H, et al. MD-2, a molecule that confers lipopolysaccharide responsiveness on Toll-like receptor 4. J Exp Med 1999; 189:1777-82.
28. Nagai Y, Akashi S, Nagafuku M, et al. Essential role of MD-2 in LPS responsiveness and TLR4 distribution. Nat Immunol 2002;3:667-72.
29. Zhang J, Rosenberg HF, Nei M. Positive Darwinian selection after gene duplication in primate ribonuclease genes. Proc Natl Acad Sci USA 1998;95:3708-13.
30. Tamura K, Dudley J, Nei M, Kumar S. MEGA4: Molecular Evolutionary Genetics Analysis (MEGA) Software Version 4.0. Mol Biol Evol 2007;24: 1596-9.
31. Smirnova I, Poltorak A, Chan EK, McBride C, Beutler B. Phylogenetic variation and polymorphism at the toll-like receptor 4 locus (TLR4). Genome Biol 2000; 1: research002.1-002.10.
32. Hajjar AM, Ernst RK, Tsai JH, Wilson CB, Miller SI. Human Toll-like receptor 4 recognizes host-specific LPS modifications. Nat Immunol 2002;3:354-9.
33. Lien E, Means TK, Heine H, et al. Toll-like receptor 4 imparts ligand-specific recognition of bacterial lipopolysaccharide. J Clin Invest 2000;105:497-504.
34. Arbour NC, Lorenz E, Schutte BC, et al. TLR4 mutations are associated with endotoxin hyporesponsiveness in humans. Nat Genet 2000;25:187-91.
35. Chamary JV, Parmley JL, Hurst LD. Hearing silence: Non-neutral evolution at synonymous sites in mammals. Nat Rev Genet 2006;7:98-108.
36. Bielawski JP, Dunn KA, Yang Z. Rates of nucleotide substitution and mammalian nuclear gene evolution. Approximate and maximum-likelihood methods lead to different conclusions. Genetics 2000;156:1299-1308.
37. Hurst LD, Williams EJ. Covariation of GC content and the silent site substitution rate in rodents: Implications for methodology and for the evolution of isochores. Gene 2000;261:107-14.
38. Bennetzen JL, Hall BD. Codon selection in yeast. J Biol Chem 1982;257:3026-31.
39. Urrutia AO, Hurst LD. The signature of selection mediated by expression on human genes. Genome Res 2003;13:2260-4.
40. Lavner Y, Kotlar D. Codon bias as a factor in regulating expression via translation rate in the human genome. Gene 2005;345:127-38.
41. Comeron JM. Selective and mutational patterns associated with gene expression in humans: Influences on synonymous composition and intron presence. Genetics 2004;167:1293-304.
42. Shen LX, Basilion JP, Stanton VP Jr. Singlenucleotide polymorphisms can cause different structural folds of mRNA. Proc Natl Acad Sci USA 1999;96:7871-6.
43. Duan J, Wainwright MS, Comeron JM, et al. Synonymous mutations in the human dopamine receptor D2 (DRD2) affect mRNA stability and synthesis of the receptor. Hum Mol Genet 2003;12:205-16.

44. Nackley AG, Shabalina SA, Tchivileva IE, et al. Human catechol-O-methyltransferase haplotypes modulate protein expression by altering mRNA secondary structure. Science 2006;314:1930-3.
45. Kimchi-Sarfaty C, Oh JM, Kim IW, et al. A "silent" polymorphism in the MDR1 gene changes substrate specificity. Science 2007;315:525-8.
46. Wasserman WW, Palumbo M, Thompson W, Fickett JW, Lawrence CE. Human-mouse genome comparisons to locate regulatory sites. Nat Genet 2000; 26:225-8.
47. Levy S, Hannenhalli S, Workman C. Enrichment of regulatory signals in conserved non-coding genomic sequence. Bioinformatics 2001;17:871-7.
48. Fickett JW, Wasserman WW. Discovery and modeling of transcriptional regulatory regions. Curr Opin Biotechnol 2000;11:19-24.
49. Frazer KA, Pachter L, Poliakov A, Rubin EM, Dubchak I. VISTA: Computational tools for comparative genomics. Nucleic Acids Res 2004:32(Web Server issue): W273-9.
50. Filipowicz W, Bhattacharyya SN, Sonenberg N. Mechanisms of post-transcriptional regulation by microRNAs: Are the answers in sight? Nat Rev Genet 2008;9:102-14.
51. Isaza R. Tuberculosis in all taxa. In Fowler ME and Miller RE, (eds.) Zoo and Wild Animal Medicine. 5th ed. Elsevier, St Louis, MO, 2003;689-96.
52. Stremlau M, Owens CM, Perron MJ, Kiessling M, Autissier P, Sodroski J. The cytoplasmic body component TRIM5a restricts HIV-1 infection in Old World monkeys. Nature 2004;427:848-53.
53. Sheehy AM, Gaddis NC, Choi JD, Malim MH. Isolation of a human gene that inhibits HIV-1 infection and is suppressed by the viral Vif protein. Nature 2002;418:646-50.
54. Rebbeck TR, Spitz M, Wu X. Assessing the function of genetic variants in candidate gene association studies. Nat Rev Genet 2004;5:589-97.
55. Ng PC, Henikoff S. SIFT: Predicting amino acid changes that affect protein function. Nucleic Acids Res 2003;31:3812-4.
56. Ramensky V, Bork P, Sunyaev S. Human non-synonymous SNPs: Server and survey. Nucleic Acids Res 2002;30:3894-900.
57. Yue P, Melamud E, Moult J. SNPs3D: Candidate gene and SNP selection for association studies. BMC Bioinformatics 2006;7:166.
58. Mi H, Guo N, Kejariwal A, Thomas PD. PANTHER version 6: Protein sequence and function evolution data with expanded representation of biological pathways. Nucleic Acids Res 2007;35(Database issue):D247-52.
59. Ferrer-Costa C, Gelpí JL, Zamakola L, Parraga I, de la Cruz X, Orozco M. PMUT: A web-based tool for the annotation of pathological mutations on proteins. Bioinformatics 2005;21:3176-8.
60. Stitziel NO, Binkowski TA, Tseng YY, Kasif S, Liang J. topoSNP: A topographic database of non-synonymous single nucleotide polymorphisms with and without known disease association. Nucleic Acids Res 2004: 32(Database issue): D520-2.
61. Stone EA, Sidow A. Physicochemical constraint violation by missense substitutions mediates impairment of protein function and disease severity. Genome Res 2005;15:978-86.
62. Thomas PD, Kejariwal A. Coding single-nucleotide polymorphisms associated with complex vs. Mendelian disease: Evolutionary evidence for differences in molecular effects. Proc Natl Acad Sci USA 2004;101:15398-403.

63. Hubbard TJ, Aken BL, Ayling S, et al. Ensembl 2009. Nucleic Acids Res 2009: 37(Database issue):D690-7.
64. Giardine B, Riemer C, Hardison RC, et al. Galaxy: A platform for interactive large-scale genome analysis. Genome Res 2005;15:1451-5.
65. Kuhn RM, Karolchik D, Zweig AS, et al. The UCSC Genome Browser Database: Update 2009. Nucleic Acids Res 2009;37(Database issue):D755-61.
66. Dewey CN. Aligning multiple whole genomes with Mercator and MAVID. Methods Mol Biol. 2007;395:221-36.
67. Tesler G. GRIMM: Genome rearrangements web server. Bioinformatics. 2002; 18:492-3.
68. Kent WJ, Baertsch R, Hinrichs A, Miller W, Haussler D. Evolution's cauldron: duplication, deletion, and rearrangement in the mouse and human genomes. Proc Natl Acad Sci USA 2003;100:11484-9.
69. Brudno M, Do CB, Cooper GM, et al. LAGAN and Multi-LAGAN: Efficient tools for large-scale multiple alignment of genomic DNA. Genome Res 2003; 13:721-31.
70. Notredame C, Higgins DG, Heringa J T-Coffee: A novel method for fast and accurate multiple sequence alignment. J Mol Biol 2000;302:205-17.
71. Do CB, Mahabhashyam MS, Brudno M, Batzoglou S. ProbCons: Probabilistic consistency-based multiple sequence alignment. Genome Res 2005:15:330-40.
72. Bray N, Pachter L. MAVID: Constrained ancestral alignment of multiple sequences. Genome Res 2004;14:693-9.
73. Marchler-Bauer A, Bryant SH. CD-Search: Protein domain annotations on the fly. Nucleic Acids Res 2004;32(W):327-31.

Cellular Immunology 259 (2009) 165–176

Contents lists available at ScienceDirect

Cellular Immunology

journal homepage: www.elsevier.com/locate/ycimm

Preliminary *in vivo* efficacy studies of a recombinant rhesus anti-$\alpha_4\beta_7$ monoclonal antibody ☆

L.E. Pereira [a], N. Onlamoon [a], X. Wang [b], R. Wang [b], J. Li [b], K.A. Reimann [b], F. Villinger [a], K. Pattanapanyasat [c], K. Mori [d], A.A. Ansari [a,*]

[a] Department of Pathology & Laboratory Medicine, Emory University School of Medicine, Room 2309 WMB, 101 Woodruff Circle, Atlanta, GA 30322, USA
[b] Division of Viral Pathogenesis, Beth Israel Deaconess Medical Center, 330 Brookline Avenue, Boston, MA 02215, USA
[c] Office for Research and Development, Department of Immunology, Faculty of Medicine, Siriraj Hospital, Mahidol University, Bangkok, Thailand
[d] AIDS Research Center, Natural Institute of Infectious Diseases, Tokyo 162-8640, Japan

ARTICLE INFO

Article history:
Received 30 April 2009
Accepted 10 June 2009
Available online 26 June 2009

Keywords:
Cell trafficking
Antibodies
AIDS
T-cells
Rhesus macaque
Act1
Alpha4beta7 integrin

ABSTRACT

Recent findings established that primary targets of HIV/SIV are lymphoid cells within the gastrointestinal (GI) tract. Focus has therefore shifted to T-cells expressing $\alpha_4\beta_7$ integrin which facilitates trafficking to the GI tract via binding to MAdCAM-1. Approaches to better understand the role of $\alpha_4\beta_7$+ T-cells in HIV/SIV pathogenesis include their depletion or blockade of their synthesis, binding and/or homing capabilities *in vivo*. Such studies can ideally be conducted in rhesus macaques (RM), the non-human primate model of AIDS. Characterization of $\alpha_4\beta_7$ expression on cell lineages in RM blood and GI tissues reveal low densities of expression by NK cells, B-cells, naïve and TEM (effector memory) T-cells. High densities were observed on TCM (central memory) T-cells. Intravenous administration of a single 50 mg/kg dose of recombinant rhesus $\alpha_4\beta_7$ antibody resulted in significant initial decline of $\alpha_4\beta_7$+ lymphocytes and sustained coating of the $\alpha_4\beta_7$ receptor in both the periphery and GI tissues.

1. Introduction

It is now established that the gut-associated lymphoid tissue (GALT) is the major initial target of pathology during acute infection of humans with HIV-1 or rhesus macaques (RM) with SIV [1–9]. During this period of primary infection, a significant frequency of CD4+ memory T-cells, which are CCR5+ and already in a state of activation due in part to exposure and response to intestinal flora, serve as prime targets for the virus leading to their infection and subsequent depletion via direct cytopathic effects and/or indirect mechanisms of apoptosis. The degree of impact of this major localized effect has been hypothesized to significantly influence the course of disease and has therefore led to a more detailed study of the mechanisms associated with T-cells that migrate and/or reside within the gastrointestinal tract. The intestinal homing receptors CCR9 and $\alpha_4\beta_7$ play one of the central roles in promoting the migration of lymphocytes into intestinal mucosal tissue via binding to CCL25 and mucosal addressin cell adhesion molecule-1 (MAdCAM), respectively [10–15]. The $\alpha_4\beta_7$ cell surface receptor has received much attention particularly in light of a recent study by Arthos et al. which demonstrated that the HIV-1 envelope protein gp120 binds to an active form of $\alpha_4\beta_7$ on CD4+ T-cells and initiates LFA-1 activation that facilitates formation of a viral synapse leading to cell-to cell spreading further facilitating viral infection [16]. Thus, the ability of the host to defend itself against lentiviral infection is likely to depend on the nature (such as phenotype and frequency) of these gut-homing lymphocytes. For instance, gut-homing virus-specific NK cells and CD8+ CTLs may contribute to the containment of HIV/SIV viral replication while gut-homing CD4+ T-cells besides their expected T helper cell activity may simply provide additional targets for the virus and sustain its replication. A detailed understanding of the immune responses in mucosal sites particularly during early stages of infection is therefore critical and because there is increasing evidence to support a significant contributing role for $\alpha_4\beta_7$+ cells in HIV pathogenesis, it is important to fully understand the part played by these cells in early viral infection and subsequent disease progression. One approach that can be taken to accomplish this aim is by conducting *in vivo* studies that utilize an anti-$\alpha_4\beta_7$ monoclonal antibody to either block $\alpha_4\beta_7$ receptor and trafficking or to deplete $\alpha_4\beta_7$+ cells prior to or during acute viral infection. This can best be studied in RM recognized to be the optimal non-human primate model for the study of AIDS. When infected with SIV, this species exhibits CD4+ T-cell depletion,

☆ Supported by NIH RO1 AI 078773-01, N0I AI 040101, R24 RR016001, grants from the Thailand Research Fund and the Ministry of Health, Labor and Welfare, Japan.

* Corresponding author.
E-mail address: pathaaa@emory.edu (A.A. Ansari).

0008-8749/$ - see front matter © 2009 Elsevier Inc. All rights reserved.
doi:10.1016/j.cellimm.2009.06.012

chronic immune activation, immune exhaustion and disease remarkably similar to HIV infection in humans [17–24]. Furthermore, the GI pathology observed in acutely HIV-infected patients is similar to the pathology exhibited by SIV-infected RM [3,7–9,25]. However, while the expression of $\alpha_4\beta_7$ on major cell lineages in humans has been documented, there is a paucity of data with regards to $\alpha_4\beta_7$-expressing cells and the effect of SIV infection on this gut-homing marker in RM. In humans, flow cytometry utilizing Act I, a murine monoclonal antibody specific for human $\alpha_4\beta_7$ integrin (henceforth referred to as murine $\alpha_4\beta_7$ mAb), showed expression of both low and high density $\alpha_4\beta_7$ ($\alpha_4\beta_7^{low}$ and $\alpha_4\beta_7^{high}$) on adult T-cells and B-cells while NK cells, eosinophils, and neonatal T- and B-cells exhibited a $\alpha_4\beta_7^{low}$ pattern of expression [10,12,26]. Furthermore, while $\alpha_4\beta_7^{low}$ was expressed by naïve T- and B-cells, $\alpha_4\beta_7^{high}$ was observed on memory T- and B-cells. Cell subsets with an $\alpha_4\beta_7^{high}$ phenotype are believed to express this receptor in an active form and are thought to be those that preferentially migrate to and following binding to their cognate MAdCAM ligand, reside within the GI tract. Several studies primarily conducted utilizing murine models have shown that the induction of $\alpha_4\beta_7^{high}$ expression on T-cells is attributed to retinoic acid (RA), which is a vitamin A metabolite catabolized specifically by either mucosal dendritic and/or stromal cells [11,15,27–32].

Thus, it was reasoned that baseline studies on the cell lineages that express $\alpha_4\beta_7$ in tissues from RM would be a pre-requisite prior to pursuing *in vivo* $\alpha_4\beta_7$+ cell-depleting and/or blocking studies in SIV-infected macaques. The purpose of the current study was therefore twofold; first, to characterize and compare $\alpha_4\beta_7$ expression levels on the major cell lineages involved in innate and adaptive immunity from healthy uninfected RM by multi-parameter flow cytometry and to evaluate the *in vitro* and *in vivo* effects of RA and SIV infection, respectively, on $\alpha_4\beta_7$ induction and/or mobilization of $\alpha_4\beta_7$+ lymphocyte subsets. Second, after acquiring a sound understanding of these factors, to conduct a preliminary safety and efficacy study of the *in vivo* administration of a monoclonal rhesus $\alpha_4\beta_7$+ antibody in RM. The results of our studies show a differential pattern of $\alpha_4\beta_7$ expression among the major cell lineages and their subsets which is similar to what has been reported for human lymphocytes. *In vitro* incubation with RA was also found to significantly induce $\alpha_4\beta_7$ expression on activated T-cells. Furthermore, while significant decreases in the frequency of $\alpha_4\beta_7$+ lymphocytes were noted in rectal biopsy tissues, no significant changes in the frequency of $\alpha_4\beta_7$+ cells were noted in the periphery of chronically SIV-infected RM. Of interest was the finding that there was a rapid disappearance of select subsets of $\alpha_4\beta_7$+ NK and $\alpha_4\beta_7$+ CD4+ T-cells in the periphery during the acute infection period. Finally, a preliminary study was conducted to define the potential *in vivo* depletion and/or blocking activity of a novel $\alpha_4\beta_7$ monoclonal antibody (modified to create a less immunogenic rhesus recombinant construct Rh-$\alpha_4\beta_7$) which was administered intravenously as a single bolus dose to healthy RM. The infusion of a single dose (50 mg/kg) of Rh-$\alpha_4\beta_7$ mAb was found to be non-toxic and lead to an initial significant decline followed by a failure to detect (up to 5 weeks) $\alpha_4\beta_7$+ lymphocytes in both peripheral and GI compartments. Collectively these data provides the foundation for *in vitro* and *in vivo* manipulation of $\alpha_4\beta_7$+ lymphocytes for potential mechanistic-based experiments in SIV-infected animals. The implications of these current findings for future studies are discussed.

2. Materials and methods

2.1. Animals

Healthy uninfected and SIV-infected RM were housed at the Yerkes National Primate Research Center (YNPRC) of Emory University. Their housing, care, diet and maintenance was in conformance to the guidelines of the Committee on the Care and Use of Laboratory Animals of the Institute of Laboratory Animal Resources, National Research Council and the Health and Human Services guidelines "Guide for the Care and Use of Laboratory Animals." The RM involved in the cross-sectional and longitudinal study were infected intravenously with 200 TCID50 of SIVmac239. All uninfected and SIV-infected RM used in the study were male and age matched adults.

2.2. Specimen collection and blood processing

Peripheral blood mononuclear cells (PBMC) were isolated by standard Ficoll–Hypaque gradient centrifugation from heparinized whole blood. This procedure in addition to those for specimen collection of and lymphocyte isolation from colon, jejunum tissues, rectal biopsies and bronchial alveolar lavage (BAL) were performed as described previously [33–35].

2.3. Viral load determination

Plasma viral loads were determined using a competitive reverse transcriptase polymerase chain reaction assay by the Virology Core Lab supported by the Emory University CFAR. To determine if the $\alpha_4\beta_7$ subset of CD4+ T-cells were preferentially infected with SIV, PBMC were isolated from the peripheral blood of 6 SIV-infected rhesus macaques during the chronic stage of infection. All monkeys were asymptomatic at the time of blood sampling. We selected three monkeys that had high (>100,000 copies/ml) and three monkeys that had low plasma viral loads (<10,000 viral copies/ml) to determine the potential role of plasma viral load on cellular viral loads in the CD4+ T-cell subsets. CD4+ T-cells were first enriched by depleting all cell lineages except CD4+ T-cells using a cocktail of monoclonal antibodies. This was followed by incubating the remaining enriched population of CD4+ T-cells with murine $\alpha_4\beta_7$ mAb at 5 μg/ml per million cells at 4 °C for 30 min. The cells were then washed and resuspended in PBS and incubated with anti-mouse Ig conjugated immuno-beads following concentrations as recommended by the commercial vendor. The enriched population of CD4+ $\alpha_4\beta_7$+ and the remaining CD4+ $\alpha_4\beta_7$− cells were then used to determine the levels of SIV. An aliquot of the CD4+ $\alpha_4\beta_7$− isolated population was subjected to flow cytometric analysis to determine degree of purity and found to contain >92% CD4+ and <0.01% $\alpha_4\beta_7$+ cells. RNA was isolated from two million cells from each of the subsets from each of the monkeys using GuHCl/Proteinase K viral lysis solution and guanidium thiocyanate carrier solution. Viral RNA was eluted in 20 μl RNAse free water and stored at −80 °C until use. Viral RNA from all the samples was then individually reverse transcribed using enhanced avian RT first strand synthesis kit and RNAse free oligoprimers (SIVgagrt). Level of viral copies were quantified in each of the cDNA sample using real time PCR using SYBR greenER for iCycler kit and the following RNAse free primer pairs:

SIV gagrt F: TTA TGG TGT ACC AGC TTG GAG GAA TGC

SIV gagrt R: CCA AAC CAA GTA GAA GTC TGT GTC TGT TCC ATC

The sensitivity of the assay was determined to be 10 viral copies/ml.

2.4. Flow cytometry

Multiple clones of monoclonal antibodies with specificity for human CD3, CD8alpha, CD8beta, CD95, CD28, alpha4 integrin (CD49d), beta7 integrin, CD16, CD14, CD20, CD56, and NKG2A, were first screened to identify those that provided optimal cross-reactivity for the identification of various T-cell, B-cell and NK cell lineages and subsets of cells from RM as described previously [33–35]. Our in-house purified and biotinylated murine $\alpha_4\beta_7$ mAb was

incubated with cells for 15 min followed by 10 min staining with PE-Cy7 or APC conjugated streptavidin for the determination of the frequency and absolute numbers of $\alpha_4\beta_7$+ lymphocytes. Stained cells fixed with 1% paraformaldehyde were analyzed on either a FACS Calibur or a LSRII flow cytometer (BD Biosciences, San Jose CA). Flow cytometric acquisition and analysis of samples as well as the gating strategy for identifying total NK cells and its subsets, the CD4+ and CD8+ T-cells subsets in lymphoid cells from rhesus macaques has been described previously [33,34].

2.5. In vitro effects of Retinoic acid (RA) on $\alpha_4\beta_7$expression

PBMC or isolated CD4+ T-cells purified by magnetic beads (Dynal Invitrogen) were cultured in RPMI 1640 media containing antibiotics and 10% fetal calf serum (heretofore referred to as media). Aliquots of such cells were cultured in media containing anti-CD3/CD28 antibody-conjugated magnetic beads [35] and/or 50 U IL-2 for 5 days at 37 °C, 5% CO_2 in the presence or absence of 10 nM all-trans RA (Sigma–Aldrich). The cells were then washed and analyzed for the frequency and relative density of $\alpha_4\beta_7$+ expression by standard flow cytometry using the FACS Calibur system.

2.6. Generation and production of rhesus recombinant $\alpha_4\beta_7$ monoclonal antibody (Rh-$\alpha_4\beta_7$ mAb)

Immunoglobulin heavy and light chain variable regions were synthesized as minigenes comprising complementarity determining regions of murine $\alpha_4\beta_7$ mAb [26], and human heavy and light chain variable region framework sequences. Synthesized variable region minigenes were subcloned into expression vectors containing rhesus IgG1 heavy chain or rhesus kappa light chain constant region sequences.

For large scale production of recombinant antibody, recombinant heavy and light chain vectors were packaged in retroviral vectors and used to infect CHO cells using the GPEx® expression technology (Catalent Pharma Solutions, Middleton, WI). A pool of transduced cells was grown in serum free medium and secreted antibody purified by protein A affinity chromatography. The purified Rh-$\alpha_4\beta_7$ mAb was placed in phosphate buffer, pH 6.5, and confirmed to contain <1 EU/mg of antibody.

2.7. Characterization of recombinant Rh-$\alpha_4\beta_7$ mAb

Specificity of Rh-$\alpha_4\beta_7$ was confirmed by cross-blocking experiments. Briefly, $\alpha_4\beta_7$+ expressing Hut 78 cells were incubated with varying concentrations of Act I or a control mouse antibody. After washing, cells were stained with the recombinant Rh-$\alpha_4\beta_7$ conjugated to the fluorophore APC. Affinity of recombinant Rh-$\alpha_4\beta_7$ was compared to the murine $\alpha_4\beta_7$ mAb by incubating serial dilutions of both antibodies with a fixed number of Hut 78 cells and measuring antibody concentration before and after incubation. The affinity constant (K_d) for each antibody was calculated as previously described [36]. Similar cross-blocking experiments were performed on PBMC isolated from uninfected RM.

2.8. Detection of cell bound Rh-$\alpha_4\beta_7$ following in vivo treatment of RM

Aliquots of PBMC and intra-epithelial lymphocytes isolated from heparinized blood and rectal biopsy samples, respectively, were stained with the biotinylated murine $\alpha_4\beta_7$ mAb followed by streptavidin PE-Cy7 to determine if the murine $\alpha_4\beta_7$ mAb binding was blocked by the Rh-$\alpha_4\beta_7$ mAb *in vivo*. To determine if decreases in levels of $\alpha_4\beta_7$+ lymphocytes as detected by the murine $\alpha_4\beta_7$ mAb were due to depletion or blocking, an aliquot of the same cells were also stained with anti-α_4 integrin-PE or anti-β_7 integrin-APC which recognize epitopes distinct from the murine $\alpha_4\beta_7$ and Rh-$\alpha_4\beta_7$ mAbs. Since α_4 integrin-PE+ lymphocytes also include $\alpha_4\beta_1$+ lymphocyte populations, the data shown herein includes staining with β_7 integrin-APC only, since cells bound by this Ab would most likely represent the same population detected by the murine $\alpha_4\beta_7$ and the Rh-$\alpha_4\beta_7$ mAbs.

2.9. Measurement of plasma levels of Rh-$\alpha_4\beta_7$

Levels of rhesus recombinant Rh-$\alpha_4\beta_7$ antibody in monkey plasma were measured using the $\alpha_4\beta_7$+ expressing CD8+ human T-cell line, HuT 78 in a flow cytometry-based assay. Plasma obtained from each monkey before and after Rh-$\alpha_4\beta_7$ mAb administration was serially diluted in PBS/2% FBS and incubated with 10^6 HuT 78 cells for 30 min. Cells were then washed twice with PBS and incubated for 30 min with polyclonal goat anti-human IgG-PE (Jackson ImmunoResearch, West Grove, PA) that had been shown to cross react with rhesus IgG. Cells were washed twice with PBS and fixed with PBS/2% formalin. Stained cells were analyzed on a FACS Calibur flow cytometer for PE fluorescence. The mean channel fluorescence intensity (MFI) of cells stained with monkey serum was compared to MFI of cells stained with known concentrations of the Rh-$\alpha_4\beta_7$ mAb. Whenever possible, the mean of two measurements made at different serum dilutions was used. The sensitivity of this assay was <4 μg/ml.

2.10. Statistical analysis

Data are represented as means ± standard deviation (SD) and were analyzed by using the two-tailed Student's *t* test. A *P* value of <0.05 was considered to be statistically significant.

3. Results

3.1. Characterization of $\alpha_4\beta_7$ expression in cell lineages from RM

Previous characterization of $\alpha_4\beta_7$ on human leukocytes using the murine Act1 mAb has shown this mAb to specifically recognize the $\alpha_4\beta_7$ heterodimer [10,26]. These studies showed that while T-cells and B-cells express both $\alpha_4\beta_7^{low}$ and $\alpha_4\beta_7^{high}$ populations, NK cells exhibited a predominantly $\alpha_4\beta_7^{low}$ phenotype. Previous studies have also examined the induction of $\alpha_4\beta_7$ expression on SIV-specific CD8+ T-cells in RM [37,38], but to date, a comprehensive analysis of profiles of $\alpha_4\beta_7$-expressing cell lineages and their subsets from RM has been lacking. Our laboratory therefore set out to first characterize $\alpha_4\beta_7$ expression profiles on T-cell and its subsets, B-cells and NK cell subsets isolated from healthy uninfected RM. Using multi-parameter flow cytometry, the biotinylated murine $\alpha_4\beta_7$ mAb was tested for reactivity along with a panel of mAb reagents that have previously been shown by several labs including ours to be optimal for the identification of the aforementioned cell populations in the PBMC samples from 9 uninfected RM. It should be noted that high and low densities of $\alpha_4\beta_7$+ expression were more discernable on the FACS Calibur flow cytometer while an overlay of histograms was necessary to better identify these two sub-populations on the LSRII flow cytometer. This is likely due to basic system differences between these two flow cytometry instruments such as laser voltages or compensation settings, but it is important to note that the frequencies of $\alpha_4\beta_7$+ lymphocytes acquired by the two flow cytometers was still similar, if not identical. As shown by the representative FACS profiles in Fig. 1A, the analysis of NK cells (defined as CD3−CD8+CD14−CD20−NKG2A+) and their subsets based on CD16 and CD56 expression [34] revealed that, in agreement with the previous characterization of human NK cells, >50% total RM NK cells generally expressed low mean densities of $\alpha_4\beta_7$ with the majority of $\alpha_4\beta_7$+ cells being the cyto-

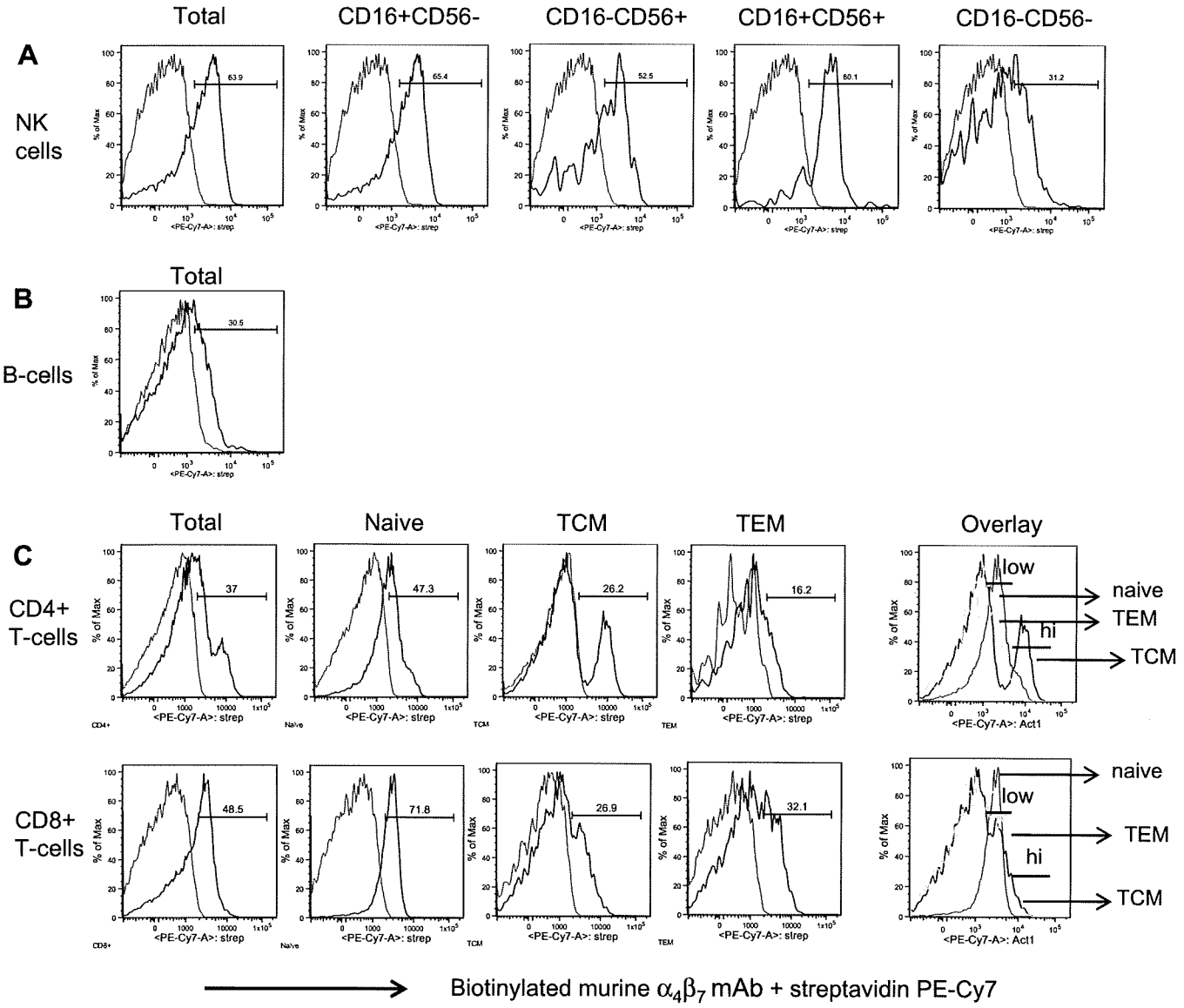

Fig. 1. Representative LSR II facilitated flow cytometric profiles of $\alpha_4\beta_7$ expression on total and subset populations of (A) NK cells, (B) B-cells and (C) T-cell lineages in PBMC from 9 healthy uninfected RM. For detection of $\alpha_4\beta_7$+ cells, PBMC from 9 RM were surface stained with biotinylated murine $\alpha_4\beta_7$ mAb followed by secondary staining with streptavidin PE-Cy7. Shown is representative data ($n = 9$ RM) with gating indicating $\alpha_4\beta_7$+ populations in comparison to background levels. To better indicate $\alpha_4\beta_7^{low}$ and $\alpha_4\beta_7^{high}$ densities, (C) also includes an overlay of $\alpha_4\beta_7$+ naïve, $\alpha_4\beta_7$+ TCM and $\alpha_4\beta_7$+ TEM for CD4+ and CD8+ T-cells.

kine-producing CD16+/CD56+ and the cytolytic CD16+CD56− NK cell subsets (Table 1). Low relative densities of $\alpha_4\beta_7$ expression were also observed on the CD16−CD56− NK cell subset in RM. In contrast to what has been reported for human B-cells, $\alpha_4\beta_7$ expression on the majority of B-cells (Fig. 1B, Table 1) in RM was found to be $\alpha_4\beta_7^{low}$. With regard to T-cells, greater than 35% of both CD4+ and CD8+ T-cells from healthy uninfected RM were found to express $\alpha_4\beta_7$ with CD4+ T-cells exhibiting both $\alpha_4\beta_7^{low}$ and $\alpha_4\beta_7^{high}$ phenotypes (Fig. 1C). Further gating based on CD28 and CD95 expression to distinguish naïve (CD28+CD95−), TCM (CD28+ CD95+) and TEM (CD28−CD95+) subsets in the periphery revealed that while there was clearly a discrete sub-population of $\alpha_4\beta_7^{high}$ expressing CD4+ TCM cells, the naïve and TEM CD4+ T-cells were $\alpha_4\beta_7^{low}$. All three (naïve, TCM and TEM) CD8+ T-cell subsets appeared to exhibit a $\alpha_4\beta_7^{low}$ phenotype (Fig. 1C). The average frequencies of $\alpha_4\beta_7$+ cells for each cell lineage and its subsets in the periphery of uninfected RM are summarized in Table 1. The examination of $\alpha_4\beta_7$ expression in intra-epithelial lymphocytes isolated from jejunum, colon and rectal tissue samples from two healthy uninfected RM (Fig. 2, representative data) revealed a predominantly $\alpha_4\beta_7^{low}$ phenotype on CD4+ T-cells, with the exception of CD4+ memory cells, which expressed heterogeneous levels of $\alpha_4\beta_7^{high}$ and were higher in frequency in the cells from the colon and rectum as compared with jejunum biopsies. CD8+ T-cells and its subsets from these tissue samples exhibited a predominantly $\alpha_4\beta_7^{low}$ phenotype (not shown).

The expression of $\alpha_4\beta_7^{high}$ on CD4+ memory T-cells has been described before and more recent studies have demonstrated that the frequency of CD4+ T-cells that express $\alpha_4\beta_7^{high}$ can be significantly increased *in vitro* via activation in the presence of retinoic acid [27,29,31], which is a vitamin A metabolite believed to be responsible for promoting the gut-homing of lymphocytes *in vivo*. In order to determine if this held true for RM T-cells, purified CD4+ T-cells were cultured *in vitro* with low levels of IL-2 and/or activated with anti-CD3/CD28 Ab-conjugated magnetic beads in the presence or absence of all-trans RA. As shown in Fig. 3A and B, flow

Table 1
Frequency (Mean ± SD) of $\alpha_4\beta_7$+ cells in major cell lineages and their subsets* in PBMC isolated from healthy uninfected RM (n = 9).

Cell sub-population	Frequency of $\alpha_4\beta_7$+ lymphocytes detected using murine $\alpha_4\beta_7$ mAb
CD3+CD4+ T-cells	51.9 ± 1.5
Na	66.7 ± 20.9
TCM	31.6 ± 6.2
TEM	18.9 ± 6.7
CD3+CD8+ T-cells	60.6 ± 16.8
Na	83.1 ± 13.4
TCM	34.4 ± 12.6
TEM	44.8 ± 15.2
CD3−CD20+ B-cells	48.5 ± 12.8
CD3−CD8+ NKG2A+ NK cells	68.2 ± 14.8
CD16−CD56+	68.7 ± 17.6
CD16+CD56−	77.4 ± 19.6
CD16−CD56−	47.0 ± 29.8
CD16+CD56+	73.2 ± 9.8

* RM lymphocytes were gated for the specific population (such as gated on CD3+CD4+ T-cells) for analysis of the frequency of $\alpha_4\beta_7$+ cells within each sub-population.

cytometric analysis on the FACS Calibur revealed that when compared to resting CD4+ T-cells, the effect of RA on $\alpha_4\beta_7$ expression was minimally enhanced when CD4+ T-cells were cultured with only IL-2. However, a dramatic increase (~4-fold) in the frequency of $\alpha_4\beta_7^{high}$ CD4+ T-cells was observed when these lymphocytes were activated in the presence of RA for 5 days. The induction of $\alpha_4\beta_7$ on CD8+ T-cells following incubation with RA was also examined but was not found to be significant, with activated cells exhibiting a less than twofold increase in the frequency of $\alpha_4\beta_7^{high}$ CD8+ T-cells in the presence of RA for 5 days (data not shown). Thus, these data collectively demonstrate that $\alpha_4\beta_7$ expression on RM lymphocytes can be readily identified and results largely reflect $\alpha_4\beta_7$ expression patterns similar to those noted for human lymphocytes. Furthermore, RA can be utilized successfully to manipulate and upregulate and potentially prepare large numbers of $\alpha_4\beta_7$+ expressing CD4+ T for autologous therapeutic transfusion studies.

3.2. In vivo administration of Rh-$\alpha_4\beta_7$ mAb results in a significant decline in the level of $\alpha_4\beta_7$+ lymphocytes in the periphery and GI tissues

The findings that the murine $\alpha_4\beta_7$ mAb effectively cross-reacts with $\alpha_4\beta_7$+ lymphocytes from RM prompted us to determine whether $\alpha_4\beta_7$-expressing lymphocytes could be targeted *in vivo*. In order to minimize the immunogenicity of the murine $\alpha_4\beta_7$ mAb *in vivo*, a rhesus recombinant IgG1 antibody was generated as noted in Section 2. The recombinant Rh-$\alpha_4\beta_7$ mAb was then confirmed by flow cytometry to exhibit specificity that was similar to murine $\alpha_4\beta_7$ mAb. The human $\alpha_4\beta_7$-expressing cell line, Hut 78, was used to characterize Rh-$\alpha_4\beta_7$ mAb. The Rh-$\alpha_4\beta_7$ mAb bound to Hut 78 cells and could be completely cross-blocked by the pre-incubation of cells with the parent murine $\alpha_4\beta_7$ mAb (Fig. 4A). The affinity constant for Rh-$\alpha_4\beta_7$ was similar to the murine $\alpha_4\beta_7$ mAb when measured by binding to Hut 78 cells with K_d values of 6.4×10^{-10} and 1.8×10^{-10} for Rh-$\alpha_4\beta_7$ mAb and murine $\alpha_4\beta_7$ mAb, respectively. The specificity of Rh-$\alpha_4\beta_7$ mAb was further confirmed by the finding that pre-incubation of RM PBMC with Rh-$\alpha_4\beta_7$ was cross-blocked the binding of murine $\alpha_4\beta_7$ mAb by almost 100% *in vitro* (and vice versa). Of interest was the finding that the pre-incubation with Rh-$\alpha_4\beta_7$ resulted in minimal cross-blocking of anti-β_7 integrin mAb (Fig. 4B) or anti-CD49d (α_4, data not shown) single chain specific mAb. Also of interest is our observation that

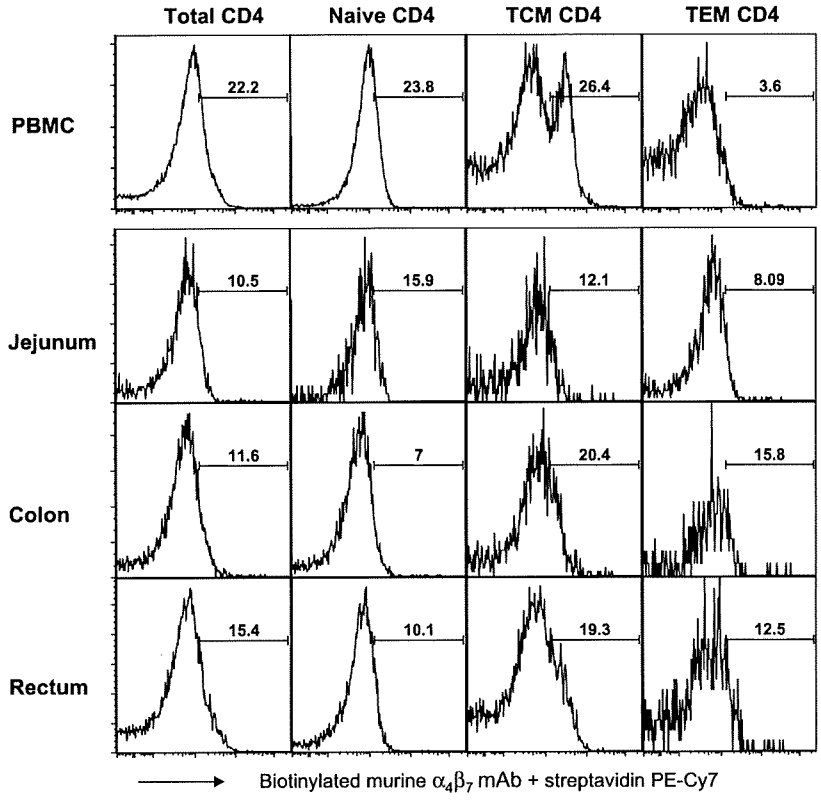

Fig. 2. Representative flow cytometric profiles of $\alpha_4\beta_7$ expression on total and subset populations of CD4+ T-cells in the gut of healthy RM. Intra-epithelial lymphocytes were isolated from colon, jejunum and rectal tissue samples from 2 healthy uninfected RM. The frequency of $\alpha_4\beta_7$+ lymphocytes were determined on the LSR II as described in the text. The number noted within each profile indicates only the frequency of cells expressing $\alpha_4\beta_7^{high}$ densities. Shown for comparison are $\alpha_4\beta_7^{high}$ populations in CD4+ T-cell subsets from uninfected RM PBMC.

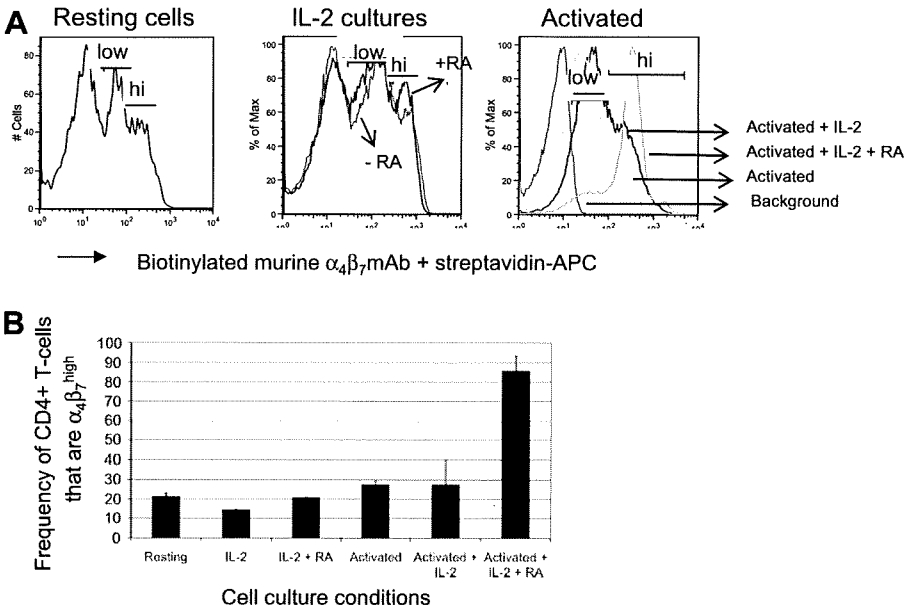

Fig. 3. Retinoic acid (RA) induces $\alpha_4\beta_7$ expression on CD4+ T-cells. (A) Representative flow cytometry profiles (acquired by the FACS Calibur) of $\alpha_4\beta_7$ expression on resting CD4+ T-cells and CD4+ T-cells cultured or activated in media containing 50 U/ml IL-2 or 10 nM retinoic acid (RA). Gating was performed on viable cells only. (B) Bar chart illustrating the frequency (Mean ± SD) of $\alpha_4\beta_7^{high}$ CD4+ T-cells under indicated conditions. The assay was repeated three times and performed using purified CD4+ T-cells from 2 RM each time.

staining with anti-β_7 integrin mAb alone did not reveal distinct low and high density β_7+ expressing CD4+ T-cell sub-populations as seen by staining with Rh-$\alpha_4\beta_7$ or murine $\alpha_4\beta_7$ mAbs. Collectively, these data suggest that the Rh-$\alpha_4\beta_7$ mAb is directed at an epitope formed by the $\alpha_4\beta_7$ heterodimer which is distinct from those that are recognized by the individual α_4 or β_7 mAbs. This finding was exploited for the detection of cells bound by Rh-$\alpha_4\beta_7$ *in vivo* (see Section 2 and below).

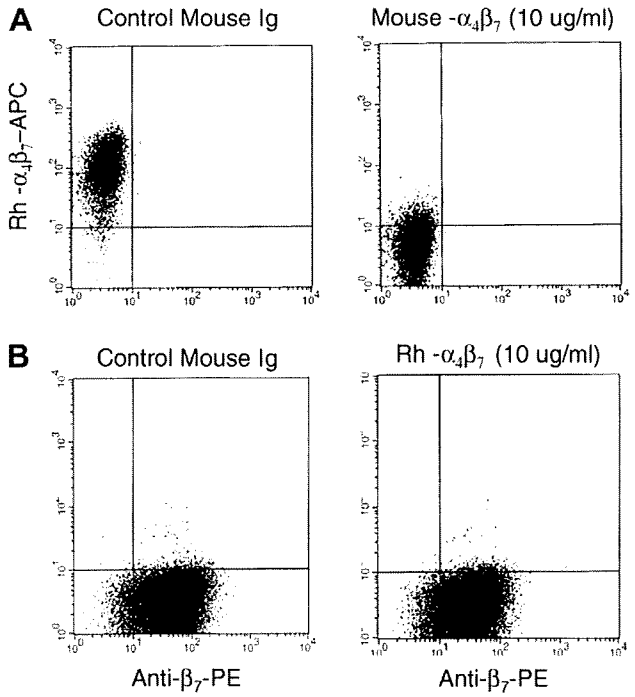

Fig. 4. Recombinant rhesus $\alpha_4\beta_7$ (Rh-$\alpha_4\beta_7$) is cross-blocked by murine $\alpha_4\beta_7$ mAb but not β_7 mAb. (A) Hut 78 cells were pre-incubated with mouse isotype control antibody (left panel), or with murine $\alpha_4\beta_7$ mAb followed by staining with Rh-$\alpha_4\beta_7$-APC. (B) Hut 78 cells were pre-incubated with mouse isotype control antibody (left panel) or with rhesus $\alpha_4\beta7$ followed by staining with β_7-PE mAb.

Having characterized the binding and specificity properties of Rh-$\alpha_4\beta_7$, an acute *in vivo* administration study was then initiated in two healthy uninfected RM RFm10 and RFn10 (6.49 and 7.17 kg, respectively). The Rh-$\alpha_4\beta_7$ mAb was diluted in sterile infusion-grade saline and was gradually administered intravenously (IV) to each of the two animals at a dose of 50 mg/kg, which equates to a starting dose of 0.85 mg/ml of plasma based on the assumption that each RM has approximately 60 ml blood/kg. The monkeys demonstrated no adverse effects during or after the antibody infusion. Blood samples used for PBMC isolation, cell blood counts (CBC) and blood chemistries were collected at baseline and at days 1, 5, 8, 14, 22, 29, 36, 43, 56 and 63 post infusion. As evident by the representative blood chemistries results (Supplemental data, Table 1), Rh-$\alpha_4\beta_7$ was well tolerated by both animals and did not lead to any significant physiological changes. The plasma levels of Rh-$\alpha_4\beta_7$ were also determined over the course of the study (see Fig. 5) and were found to be at a maximum as expected on Day 1 (603 and 676 μg/ml in RFm10 and RFn10, respectively) followed by a decline thereafter with an alpha half life of approximately 8 days. By day 29, notable concentrations were still detected in plasma from both RFm10 (45 μg/ml) and RFn10 (35 μg/ml) but undetectable levels were noted by day 56.

PBMC were analyzed by flow cytometry to determine the frequency of major $\alpha_4\beta_7$+ cell lineages and their subsets. Detection of $\alpha_4\beta_7$+ cells following *in vivo* administration of the Rh-$\alpha_4\beta_7$ using the parent murine $\alpha_4\beta_7$ mAb alone would not be feasible due to cross-blocking. Attempts were made to directly detect Rh-$\alpha_4\beta_7$ on PBMC utilizing PE-conjugated anti-rhesus IgG. However, despite Fc blocking prior to *in vitro* staining, the background level with this secondary antibody was too high to allow for clear identification of cells bound by the Rh-$\alpha_4\beta_7$ (data not shown). Based on the findings that the Rh- $\alpha_4\beta_7$ mAb does not block the reactivity of mAb against either the α_4 intergrin or β_7 integrin single chain, it was reasoned that use of the anti-β_7 integrin mAb would be preferable since the anti-α_4 integrin mAb would not only bind to cells with bound Rh-$\alpha_4\beta_7$ but would also bind to cells that express $\alpha_4\beta_1$. It was thus reasoned that the detection of cells that are β_7+ would likely represent cells that are bound with the Rh-$\alpha_4\beta_7$ mAb *in vivo*. Thus, the frequency of $\alpha_4\beta_7$+ cells was determined by staining aliquots of

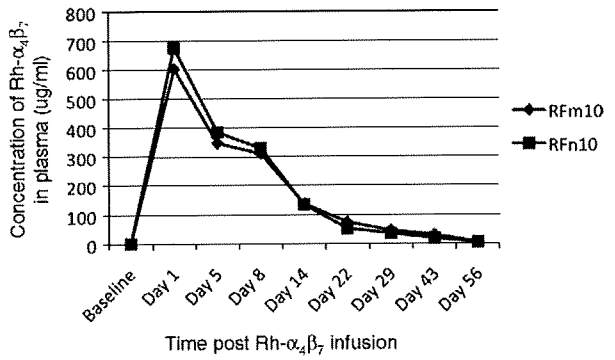

Fig. 5. Plasma concentrations of Rh-$\alpha_4\beta_7$ following *in vivo* infusion. Plasma was isolated from heparinized blood at the indicated time points from animals RFm10 and RFn10 and the levels of Rh-$\alpha_4\beta_7$ mAb were measured using the $\alpha_4\beta_7$+ expressing CD8+ human T-cell line HuT 78 in a flow cytometry-based assay. The concentration of Rh-$\alpha_4\beta_7$ in each plasma sample was determined by comparing the MFI of HuT 78 cells stained with monkey plasma to the MFI of HuT 78 cells stained with known concentrations of Rh-$\alpha_4\beta_7$ mAb.

cells with the parent murine $\alpha_4\beta_7$ mAb as well as with anti-β_7 chain specific mAb. Results revealed that on Day 1 post infusion, there was significant cross-blocking of $\alpha_4\beta_7$+ T-cells and α_4v_7+ NK cells by Rh-$\alpha_4\beta_7$ mAb because staining of PBMC with the parent murine $\alpha_4\beta_7$ mAb showed a decline in frequency by ~95% while the decline in the frequency of $\alpha_4\beta_7$+ B-cells was by ~80% in both the monkeys (Fig. 6A, upper left panel). This decline occurred in both $\alpha_4\beta_7^{low}$ and $\alpha_4\beta_7^{high}$ subsets. The frequency of $\alpha_4\beta_7$+ lymphocytes remained low through Day 22 until a significant increase to levels near baseline were noted by Day 43.

To distinguish between cross-blocking and a true decline in $\alpha_4\beta_7$+ lymphocytes, staining with anti-β_7 mAb was performed and also revealed a similar decline in β_7+ lymphocytes on Day 1 post infusion (Fig. 6A, lower left panel). However, this was followed by a rebound to ~60–70% of baseline on Day 5. These increased values were maintained until day 22 with values returning near baseline by Day 36. These data suggest that while there is an initial and partial decline in the $\alpha_4\beta_7$+ expressing cells, this is followed by a recovery of cells that express $\alpha_4\beta_7$+ but are blocked by the *in vivo* presence of the Rh-$\alpha_4\beta_7$ mAb. The absolute

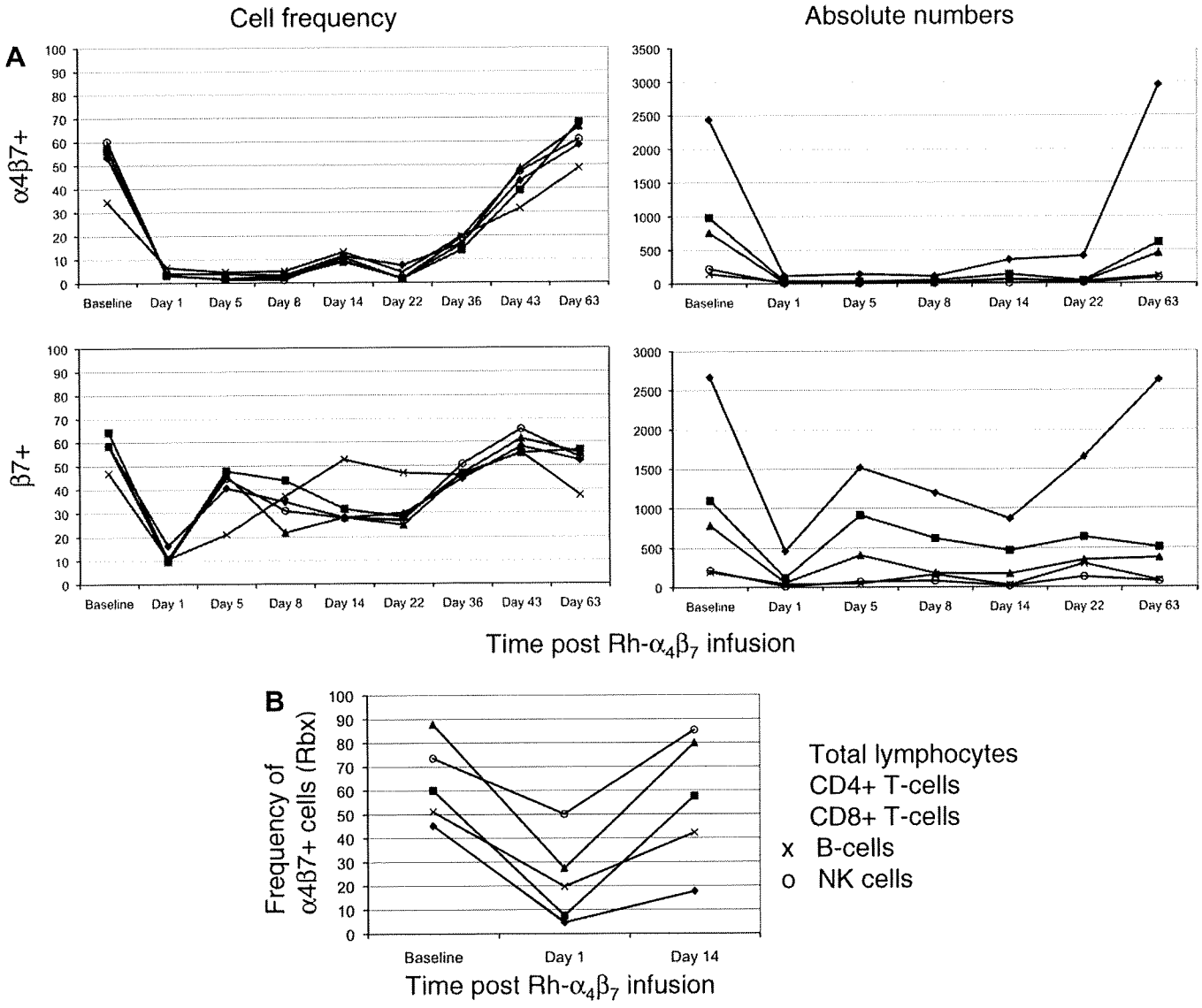

Fig. 6. *In vivo* administration of Rh-$\alpha_4\beta_7$ leads to significant decline and subsequent cross-blocking of $\alpha_4\beta_7$+ lymphocytes. Rh-$\alpha_4\beta_7$ was infused IV at a dose of 50 mg/kg to 2 RM and the frequency and ABS of $\alpha_4\beta_7$+ and β_7+ lymphocytes for each cell lineage in (A) the periphery and (B) Rbx, were determined at the indicated points post infusion. Shown is representative data for total $\alpha_4\beta_7$+ lymphocytes (♦), $\alpha_4\beta_7$+ CD4+ T-cells (■), $\alpha_4\beta_7$+ CD8+ T-cells (▲), $\alpha_4\beta_7$+ B-cells (x), and $\alpha_4\beta_7$+ NK cells (o).

numbers (ABS) of total lymphocytes, CD4+ T-cells, CD8+ T-cells, B-cells and NK cells expressing $\alpha_4\beta_7$+ and β_7+ (Fig. 6A, right panels) were also calculated in order to distinguish whether the observed decreases in cell frequency were due to the cross-blocking effects of Rh-$\alpha_4\beta_7$ mAb or was due to a true decrease (depletion or re-distribution). As shown by the representative data in Fig. 6A, the analysis of ABS of $\alpha_4\beta_7$+ and β_7+ T-cells, B-cells and NK cells revealed a true decline in these cell populations in the periphery on Day 1 which reflects the cell frequency data. By day 63, the ABS of all these lymphocyte subsets returned to baseline levels.

Since $\alpha_4\beta_7$+ lymphocytes home to the GI tract which is the target site of interest, the frequency of $\alpha_4\beta_7$+ and β_7+ lymphocytes was also determined in rectal biopsy (Rbx) samples from each animal at baseline, Day 1 and Day 14 post infusion with the Rh-$\alpha_4\beta_7$ mAb. A similar analysis of BM and BAL samples was also performed to determine the extent of Rh-$\alpha_4\beta_7$ bio-distribution *in vivo*. As shown by the results in Fig. 6B, staining of isolated day 1 Rbx intra-epithileal lymphocytes with either the murine $\alpha_4\beta_7$ mAb or the anti-β_7 integrin mAb revealed a 10-fold and 3-fold decline in the frequency of $\alpha_4\beta_7$+ CD4+ T-cells and $\alpha_4\beta_7$+ CD8+ T-cells, respectively. An approximately 2-fold decrease was also noted for $\alpha_4\beta_7$+ B-cells and $\alpha_4\beta_7$+ NK cells in such Rbx tissues. By Day 14, the frequencies of all $\alpha_4\beta_7$+ lymphocyte populations were at or near baseline. A similar pattern of decrease in the frequency of $\alpha_4\beta_7$+ lymphocytes was noted for bone marrow samples in that significant declines in $\alpha_4\beta_7$+ lymphocytes were observed on Day 1 while a recovery to levels near baseline were noted on Day 14. Data obtained from BAL samples did not reveal any clear trend (data not shown). In summary, *in vivo* administration of a single dose of 50 mg/kg of Rh-$\alpha_4\beta_7$ was well tolerated and resulted in significant initial decline and a prolonged blocking of the $\alpha_4\beta_7$ molecule on peripheral $\alpha_4\beta_7$+ T-cells, B-cells and NK cells for a significant period of time (up to 5 weeks) as well as a substantial decrease in the frequency of these lymphocyte subsets in Rbx and BM samples, but for a more transient time period.

3.3. Cross-sectional and longitudinal analyses of uninfected and SIV-infected RM reveals early changes in the frequency and absolute numbers (ABS) of select $\alpha_4\beta_7$+ lymphocyte subsets during the acute stage of infection

Since our main goal is to eventually administer the Rh-$\alpha_4\beta_7$ mAb to RM prior to or during acute SIV-infection, it was deemed important to first characterize and understand the changes, if any, that occur in $\alpha_4\beta_7$+ lymphocytes following SIV-infection. To this end, both longitudinal and cross-sectional studies were conducted to evaluate the acute and chronic effects, respectively, of SIV-infection on $\alpha_4\beta_7$+ expression on lymphocytes from the periphery and GI tissues of uninfected and SIV-infected RM. The cross-sectional analysis of PBMC samples from SIVmac239 chronically infected RM ($n = 9$) with either high VL (>100,000 vRNA copies/ml plasma, $n = 5$) or low VL (<10,000 vRNA copiles/ml plasma, $n = 4$) and for comparison uninfected RM ($n = 5$) failed to reveal any significant changes ($p > 0.05$) in the frequency of $\alpha_4\beta_7$+ T-cell subsets, $\alpha_4\beta_7$+ B-cells or $\alpha_4\beta_7$+ NK cell subsets in samples from the SIV-infected animals during chronic infection as compared to the uninfected control animals (data not shown). However, the comparison of intra-epithelial lymphocytes isolated from Rbx from 2 uninfected and 2 SIV-infected RM 8–10 weeks post infection revealed a $\geqslant$2-fold decline in the frequency of $\alpha_4\beta_7$+ NK cells and $\alpha_4\beta_7$+ T-cells particularly among $\alpha_4\beta_7$+ CD4+ TEM cells and $\alpha_4\beta_7$+ CD8+ T-cells (Fig. 7) while a relatively smaller decline was noted for $\alpha_4\beta_7$+ B-cells in these Rbx tissues. The relative viral loads in enriched populations of $\alpha_4\beta_7$+ versus $\alpha_4\beta_7$– enriched CD4+ T-cell populations isolated from the peripheral blood of 6 chronically SIV-infected but asymptomatic RM with both high and low ($n = 3$ each) plasma VL was also determined but results revealed no statistically significant differences in cellular VL copy number between the $\alpha_4\beta_7$+ and $\alpha_4\beta_7$– CD4+ T-cells ($p > 0.05$, data not shown).

In contrast to chronically SIV-infected RM, significant changes in the frequency and ABS of select peripheral T-cell and NK cell subsets were noted during the acute phase of SIV-infection. Analysis of 4 RM prior to (following two consecutive baseline values) and during the first 5 weeks of infection with SIVmac239 revealed that a significant increase in both the frequency (Fig. 8A, left panel) and ABS (not shown) of total NK cells occurred in the periphery which is similar to our previous findings [34]. Analysis of the specific $\alpha_4\beta_7$+ NK cells and its subsets (Fig. 8A, right panel) revealed that a nearly 4-fold decline occurred in the frequency of $\alpha_4\beta_7$+ CD16–CD56+ and $\alpha_4\beta_7$+ CD16–CD56– NK subsets at week 1 post infection while a less significant decline was also noted in the frequency of $\alpha_4\beta_7$-expressing CD16+CD56– and CD16+CD56+ NK subsets. The determination of absolute numbers (ABS) revealed an approximate 2-fold decline by week 2 and the ABS of the $\alpha_4\beta_7$+ CD16–CD56+ and $\alpha_4\beta_7$+ CD16–CD56– NK subsets remained low through week 5 (not shown). However, a substantial increase in the ABS of $\alpha_4\beta_7$+ CD16+CD56– and CD16+CD56+ NK subsets was observed, with a 4-fold and 2-fold increase, respectively, being

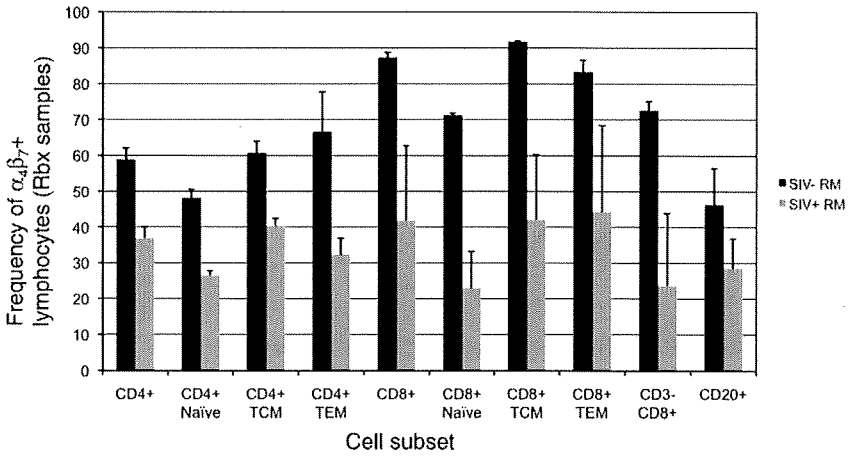

Fig. 7. Chronic SIV infection in RM leads to a decline in the frequency of most $\alpha_4\beta_7$+ lymphocytes in the GALT. Intra-epithelial lymphocytes isolated from rectal biopsy samples from uninfected (black bars, $n = 2$) and SIV-infected rhesus macaques (grey bars, $n = 2$, approximately 2 mths post infection) were stained with biotinylated murine $\alpha_4\beta_7$ mAb and streptavidin-PE-Cy7 and analyzed by flow cytometry. Shown are the frequency of $\alpha_4\beta_7$+ cells within CD4+ and CD8+ T-cell subsets, NK cells and B-cells.

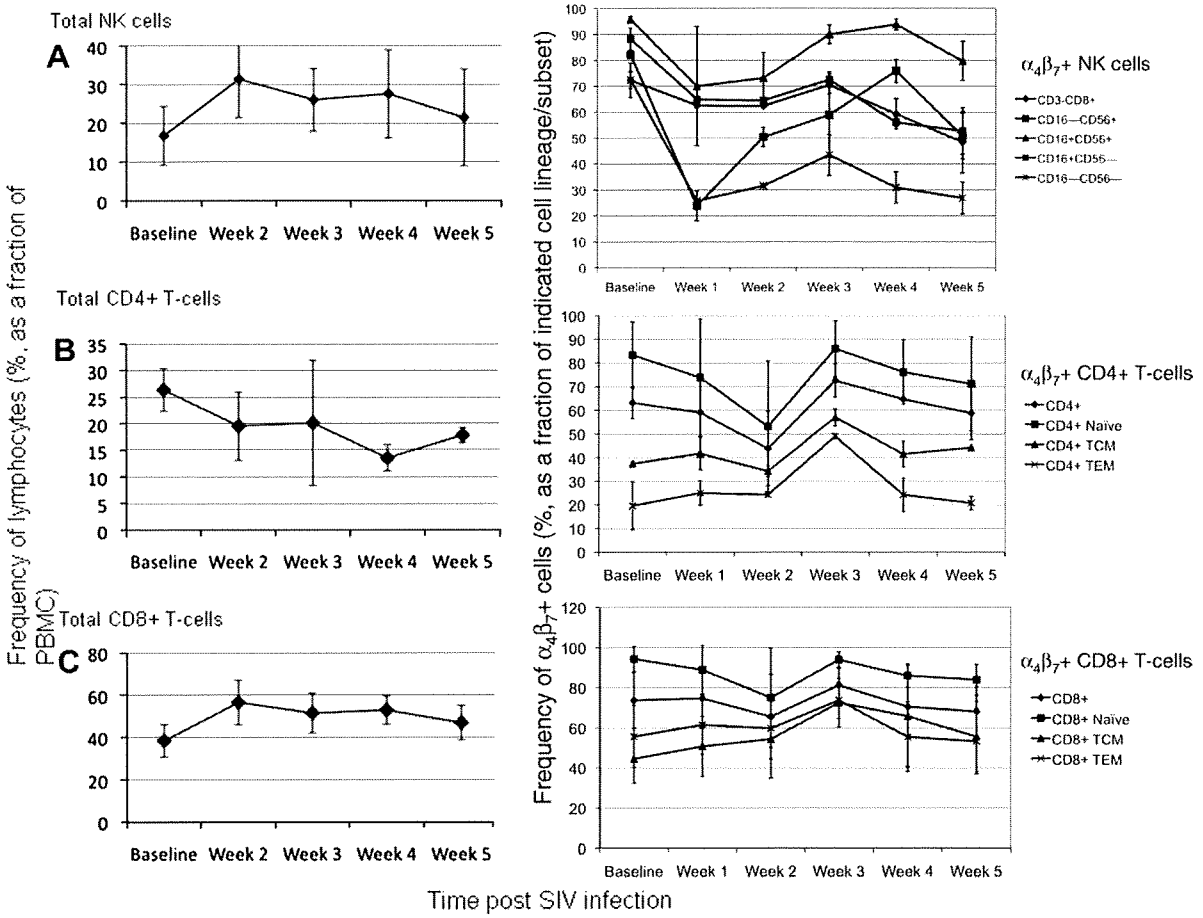

Fig. 8. Acute SIV infection in RM leads to a decline and/or mobilization of select $\alpha_4\beta_7$+ lymphocytes. Longitudinal analysis of the frequency of (A) total and $\alpha_4\beta_7$+ NK cell subsets, (B) total and $\alpha_4\beta_7$+ CD4+ T-cell subsets and (C) total and $\alpha_4\beta_7$+ CD8+ T-cell subsets during the acute phase of SIV infection in RM. The frequency of total NK cells, CD4+ T-cells and CD8+ T-cells (left panels) was determined in 4 RM that were experimentally infected with SIVmac239. Isolated PBMC were also stained with biotinylated murine $\alpha_4\beta_7$ mAb followed by streptavidin PE-Cy7 and the frequencies of indicated $\alpha_4\beta_7$+ lymphocyte subsets (right panels) in the periphery were monitored by flow cytometry every week for 5 weeks post infection. Shown are the mean frequencies for each cell subset at the indicated time points. Changes, if any, in ABS are described in the text.

noted at week 2 post infection. Levels of ABS returned to near baseline values for the cytolytic $\alpha_4\beta_7$+ CD16+CD56− NK subset by week 5 but remained elevated for $\alpha_4\beta_7$+ CD16+CD56+ NK cells.

With regards to CD4+ T-cells, a steady decline in the frequency of total CD4+ T-cells was observed (Fig. 8B, left panel) and while a 20–30% decrease in the frequency of total $\alpha_4\beta_7$+ CD4+ T-cells and the $\alpha_4\beta_7$+ naïve subset was observed by week 2, no significant changes were noted in the frequency of $\alpha_4\beta_7$+ TCM and $\alpha_4\beta_7$+ TEM subsets (Fig. 8B, right panel). However, the analysis of ABS at week 2 revealed a significant 2–3-fold decline in all three $\alpha_4\beta_7$+ CD4+ T-cell subsets with the largest decrease being observed for $\alpha_4\beta_7$+ naïve and $\alpha_4\beta_7$+ TCM subsets (data not shown). The levels of these subsets remained low with a modest increase in ABS being observed at week 5 post infection. No significant changes in the frequency of $\alpha_4\beta_7$+ CD8+ T-cells and its $\alpha_4\beta_7$+ subsets were observed during the acute infection period (Fig. 8C, right panel). However, in contrast to $\alpha_4\beta_7$+ CD4+ T-cells, a slight increase in the ABS of $\alpha_4\beta_7$+ CD8+ T-cells and its subsets were noted at week 2 post infection, with the largest increase (2-fold) being noted for the $\alpha_4\beta_7$+ TEM subset (data not shown). The ABS of the $\alpha_4\beta_7$+ CD8+ TCM subset remained steady but by weeks 4 and 5, an approximately 2-fold decline in the ABS of the $\alpha_4\beta_7$+ CD8+ naïve and $\alpha_4\beta_7$+ CD8+ TEM subsets were observed. There were no significant changes observed in the frequency of $\alpha_4\beta_7$+ B-cells and there was no clear trend noted in ABS of B-cells during acute SIV-infection (data not shown).

4. Discussion

The implications of $\alpha_4\beta_7$ expression patterns on the ability of distinct cell populations to home to gut mucosal sites have led to efforts to understand both the mechanism behind the substantial decline in CD4+ T-cells in HIV/SIV pathogenesis as well as mechanisms underlying the trafficking of lymphocytes that would naturally replace and potentially help in the control of viral replication at this site of infection. A recent study by Arthos et al. [16] demonstrated that not only was there a direct interaction between $\alpha_4\beta_7$ and the HIV envelope protein gp120 but that depending on the viral isolate, there was considerable variability in the efficiency with which this binding occurred. Thus, in addition to offering one explanation for the rapid decline in mucosal memory CD4+ T-cells during acute HIV infection, these observations also raise the possibility that targeting gp120-$\alpha_4\beta_7$ interactions *in vivo* may interfere with optimal binding, perhaps limiting and/or inhibiting the establishment of a successful viral infection. Studies of *in vivo* blocking studies in mice using antibodies against $\alpha_4\beta_7$ have already laid the foundation for blocking such receptor ligand interactions in the trafficking of T-cells to intestinal tissues [39,40]. Several antagonists for the gut-homing markers $\alpha_4\beta_7$ and even CCR9 are currently in clinical development for the treatment of inflammatory diseases, which include humanized anti-$\alpha_4\beta_7$ antibody and the use of a small molecule CCR9 inhibitor such as Traficet-EN™ (ChemoCentryx) for the treatment of Crohn's disease and ulcera-

tive colitis [41,42]. Exploiting this approach in the context of HIV pathogenesis may prove to be effective since an anti-$\alpha_4\beta_7$ blocking or depleting antibody may have preventative or therapeutic effects. Given the limitations of our knowledge of the potential consequences that such therapy would have in HIV patients, the studies presented herein therefore set out to first characterize $\alpha_4\beta_7$ expression patterns in RM, the non-human primate model of AIDS, and then proceeded to evaluate the safety and efficacy of a Rh-$\alpha_4\beta_7$ mAb which is a recombinant primatized construct of the original murine $\alpha_4\beta_7$ mAb that has previously been shown to specifically recognize the $\alpha_4\beta_7$ heterodimer.

While the analysis of $\alpha_4\beta_7$ expression on various lymphocyte subsets from RM revealed expression patterns that are basically very similar to what has been reported for human lymphocytes, some notable differences were observed. First, $\alpha_4\beta_7$ expression levels on CD8+ T-cells and particularly B-cells in RM were predominantly low which is in contrast to what has been observed on these two lymphocyte subsets in humans. This may possibly be due to a species-specific difference although it should be noted that even in humans, considerable variability in $\alpha_4\beta_7$ density was reported at least for B-cells and this appeared to be age-related [10]. Second, our results showed that $\alpha_4\beta_7^{high}$ is expressed on mostly peripheral CD4+ TCM T-cells (as defined by CD28, CD95 and CCR7 expression) with CD4+ naïve and TEM cells being predominantly $\alpha_4\beta_7^{low}$, and only a small frequency of $\alpha_4\beta_7^{high}$ CD4+ cells were observed in GALT samples which was unexpected. These observations raise the question of whether high densities of $\alpha_4\beta_7$ are truly required for mobilization to the gut or if significant down-regulation of $\alpha_4\beta_7$ expression occurs after $\alpha_4\beta_7$+ lymphocytes have trafficked to this mucosal target site. More detailed trafficking studies of $\alpha_4\beta_7^{low}$ and $\alpha_4\beta_7^{high}$ lymphocytes will be required to better address this issue. Nonetheless, our observation of $\alpha_4\beta_7^{high}$ expression levels on predominantly CD4+ memory T-cells in combination with the recent finding by Arthos et al. regarding the binding of HIV gp120 to $\alpha_4\beta_7$, offers further support for why this cell subset is relatively more susceptible to infection and depletion early in infection. However, our analysis of cellular VL in purified $\alpha_4\beta_7$+ and $\alpha_4\beta_7$− CD4+ T-cell populations from chronically SIV-infected RM suggest no preferential replication of SIV in $\alpha_4\beta_7$+ cells over $\alpha_4\beta_7$− subsets although studies are being pursued by us to determine cellular VL in more specific $\alpha_4\beta_7^{low}$ and $\alpha_4\beta_7^{high}$ subsets, particularly in acutely SIV-infected animals, to elucidate the susceptibility of these cell populations to infection and subsequent depletion. Replacing this depleted population via infusion methods is not implausible as our current study showed that high levels of $\alpha_4\beta_7$ expression on CD4+ T-cells can be effectively induced *in vitro* with RA. Thus, expanding these cells *ex vivo* for possible *in vivo* infusion experiments as a means to replenish CD4+ T-cells and/or provide robust effector CD4+ T-cells that home preferentially to the affected GI compartment is feasible. In support of this, a recent study that involved the *in vivo* tracking of infused CFSE-labeled CD4+ $\alpha_4\beta_7$+ T-cells that were expanded *ex vivo* with anti-CD3/CD28 Abs revealed that the gut tissues contained 2% of such labeled cells at 1 week following infusion (Villinger et al., manuscript in preparation). While results of the *in vitro* RA assay did not reveal any significant induction of $\alpha_4\beta_7$ expression on CD8+ T-cells following a 5-day incubation period with RA, it is possible that the kinetics of $\alpha_4\beta_7$ upregulation on this cell lineage may be delayed in comparison to CD4+ T-cells and prolonged treatment with this Vitamin A metabolite may lead to significant $\alpha_4\beta_7$ induction on CD8+ T-cells.

Our analysis of $\alpha_4\beta_7$ expression in the context of SIV infection revealed rapid peripheral declines in select lymphocyte subsets that include $\alpha_4\beta_7$+ CD4+ T-cells and $\alpha_4\beta_7$+ NK cells primarily during the acute phase. It is not clear whether these rapid peripheral declines in $\alpha_4\beta_7$+ CD4+ T-cells are due to induced trafficking to the GALT, direct cytopathic effects of the virus, or both. Of importance, the declines in peripheral $\alpha_4\beta_7$+ NK cells, particularly within the cytokine-producing $\alpha_4\beta_7$+ CD16−CD56+ subset, suggest that their trafficking to the GI track is induced as early as week 1, setting in motion downstream SIV-specific adaptive immune responses at this major site of infection. In support of this view, a decline in the ABS of $\alpha_4\beta_7$+ naïve and $\alpha_4\beta_7$+ TEM CD8+ T-cells occurred in the periphery at weeks 4 and 5, after the noted decline in $\alpha_4\beta_7$+ CD16−CD56+ NK cells. If trafficking of $\alpha_4\beta_7$+ NK cells to the GALT is indeed occurring, this again raises the question of whether high densities of $\alpha_4\beta_7$ expression are truly required for trafficking to this mucosal site since NK cells in RM were found to exhibit primarily a $\alpha_4\beta_7^{low}$ phenotype, as did CD8+ TEM cells. It is possible that integrins other than $\alpha_4\beta_7$ contribute to trafficking of certain cell lineages to the GI tract. It is of interest to note that there were minimal changes in the level of $\alpha_4\beta_7$+ B-cells during acute SIV infection, suggesting a less prominent role for this cell lineage in the GALT or that other gut-homing receptors are upregulated on B-cells during acute SIV/HIV infection.

Prior to *in vivo* administration of Rh-$\alpha_4\beta_7$ mAb, we confirmed that this mAb had limited immunogenicity to minimize cellular activation that could lead to additional cellular targets for SIV infection therefore counteracting the intended preventive or therapeutic effect of the antibody in future experiments with SIV-infected RM. Experiments to evaluate the effect of this antibody on general tyrosine phosphorylation in unfractionated PBMC or highly enriched population of CD4+ T-cells failed to reveal any detectable increase in phosphorylation when compared to untreated cells (data not shown). An additional *in vitro* ^{3}H-thymidine-based cell proliferation assay revealed that Rh-$\alpha_4\beta_7$ at varying concentrations (0.1–25 μg/ml) failed to induce detectable cell proliferation (data not shown), thus lending further support for the observation that Rh-$\alpha_4\beta_7$ does not induce detectable levels of cell activation at least under these conditions. These data are distinct from a previous study [43] which reported that immobilized $\alpha_4\beta_7$ mAb served to co-stimulate T-cells when used in conjunction with sub-mitogenic doses of anti-CD3 mAb. Similar approaches are therefore being pursued in efforts to determine if in fact our Rh-$\alpha_4\beta_7$ mAb has similar effects. The administration of Rh-$\alpha_4\beta_7$ *in vivo*, even at a high dose of 50 mg/kg was however well tolerated. Importantly, the substantial decline in the frequency and ABS of $\alpha_4\beta_7$+ lymphocytes in both the periphery and GALT on Day 1 suggests that Rh-v$_4\beta_7$ successfully exerted its effect *in vivo*. Although the reduction in ABS and frequency of $\alpha_4\beta_7$+ lymphocytes in the periphery and GALT, respectively, suggests a true decline in these cell populations, the redistribution of these lymphocytes to other compartments cannot be ruled out. For future experiments, it would also be important to determine if such a decrease in ABS also occurs in the GALT following Rh-$\alpha_4\beta_7$ administration.

During the course of this experiment, two additional observations were made which provided important information about both the mAb itself and the nature of the cells that it targets. First, a recovery of β_7 integrin+ lymphocytes was noted in the periphery at Day 5 and thereafter but the level of $\alpha_4\beta_7$+ lymphocytes detected by murine $\alpha_4\beta_7$ mAb was still negligible for >6 weeks after Rh-$\alpha_4\beta_7$ administration, suggesting that circulating Rh-$\alpha_4\beta_7$ cross-blocked newly produced and/or newly trafficking $\alpha_4\beta_7$+ cells upon entry into the periphery thereby blocking their detection by the murine mAb. The finding that the primatized mAb remained in circulation for up to 40–50 days also suggests long-term *in vivo* stability and that it was unlikely that the monkeys generated an immune response to this antibody, which otherwise would have exhibited a faster *in vivo* clearance. Second, our results also revealed that the extent of decline was not uniform among the cell lineages, with a slightly less pronounced decrease being noted for $\alpha_4\beta_7$+ B-cells in the periphery and GALT. It is possible that differences in the tissue

specific redistribution of these cell lineages and/or rates of cell turnover account for this difference, since it has been reported that B-cell turnover in RM occurs at a rate faster than T-cells [44,45]. Thus, the observed lower level of decline of $\alpha_4\beta_7$+ B-cells may be due to quicker neogenesis/replacement of these lymphocytes and perhaps a more substantial decrease may have been observed in the hours immediately following Rh-$\alpha_4\beta_7$ administration. Nonetheless, these data collectively demonstrate that Rh-$\alpha_4\beta_7$ can be safely administered and results in remarkably efficient cross-blocking of the $\alpha_4\beta_7$ receptor and perhaps even a decline due to redistribution and/or depletion of $\alpha_4\beta_7$+ lymphocytes, particularly T-cells which ultimately is the target cell lineage of interest. These observations lay the foundation for future chronic dosing experiments with Rh-$\alpha_4\beta_7$ in acutely and chronically SIV-infected animals. Whether chronic dosing of this mAb leads to safe and sustained cross-blocking, depletion and/or redistribution of $\alpha_4\beta_7$+ lymphocytes remains to be determined and is the current focus of study in our laboratory, as are studies to determine the potential preventative and/or therapeutic effects of Rh-$\alpha_4\beta_7$ during early viral infection.

Acknowledgments

We thank Dr. James T. Kurnick who provided us with the murine $\alpha_4\beta_7$ mAb clone and also thank Stephanie Ehnert and the veterinary and support staff of the YNPRC for their efficient care and handling of the animals. We also thank Ann Mayne, Susan Stephenson, Austin Lewis, Dawn Little and Keli Kolegraff for their help with initial characterization of the murine $\alpha_4\beta_7$ mAb.

Appendix A. Supplementary data

Supplementary data associated with this article can be found, in the online version, at doi:10.1016/j.cellimm.2009.06.012.

References

[1] S. Dandekar, Pathogenesis of HIV in the gastrointestinal tract, Current HIV/AIDS Reports 4 (2007) 10–15.
[2] M. Guadalupe, E. Reay, S. Sankaran, T. Prindiville, J. Flamm, A. McNeil, S. Dandekar, Severe CD4+ T-cell depletion in gut lymphoid tissue during primary human immunodeficiency virus type 1 infection and substantial delay ini restoration following highly active antiretroviral therapy, J. Virol. 77 (2003) 11708–11717.
[3] C. Heise, P. Vogel, C.J. Miller, C.H. Halsted, S. Dandekar, Simian immunideficiency virus infection of the gastrointestinal tract of rhesus macaques. Functional, pathological and morphological changes, Am. J. Pathol. 142 (1993) 1759–1771.
[4] R.P. Johnson, How HIV guts the immune system, N. Engl. J. Med. 358 (2008) 2287–2289.
[5] S. Mehandru, M.A. Poles, K. Tenner-Racz, P. Jean-Pierre, V. Manuelli, P. Lopez, A. Shet, A. Low, H. Mohri, D. Boden, P. Racz, M. Markowitz, Lack of mucosal immune reconstitution during prolonged treatment of acute and early HIV-1 infection, PLoS Med. 3 (2006) 2335–2348.
[6] A.H. Talal, C.E. Irwin, D.T. Dieterich, H. Yee, L. Zhang, Effect of HIV-1 infection on lymphocyte proliferation in gut-associated lymphoid tissue, J. Acquir. Immune. Defic. Syndr. 26 (2001) 208–217.
[7] M. Vajdy, R. Veazey, I. Tham, C. deBakker, S. Westmoreland, M. Neutra, A. Lackner, Early immunologic events in mucosal and systemic lymphoid tissues after intrarectal inoculation with simian immunodeficiency virus, J. Infect. Dis. 184 (2001) 1007–1014.
[8] M. Vajdy, R.S. Veazey, H.K. Knight, A.A. Lackner, M.R. Neutra, Differential effects of simian immunideficiency virus infection on immune inductive and effector sites in the rectal mucosa of rhesus macaques, Am. J. Pathol. 157 (2000) 485–495.
[9] R.S. Veazey, M. DeMaria, L.V. Chalifoux, D.E. Shvetz, D.R. Pauley, H.L. Knight, M. Rosenzweig, R.P. Johnson, R.C. Desrosiers, A.A. Lackner, Gastrointestinal tract as a major site of CD4+ T cell depletion and viral replication in SIV infection, Science 280 (1998) 427–431.
[10] D.J. Erle, M.J. Briskin, E.C. Butcher, A. Garcia-Pardo, A.I. Lazarovits, M. Tidswell, Expression and function of the MAdCAM-1 receptor, integrin $\alpha_4\beta_7$, on human leukocytes, J. Immunol. 153 (1994) 517–527.
[11] J.R. Mora, M.R. Bono, N. Manjunath, W. Weninger, L.L. Cavanagh, M. Rosemblatt, U.H.V. Andrian, Selective imprinting of gut-homing T-cells by Peyer's patch dendritic cells, Nature 424 (2003) 88–93.
[12] L.S. Rott, M.J. Briskin, D.P. Andrew, E.L. Berg, E.C. Butcher, A fundamental subdivision of circulating lymphocytes defined by adhesion to mucosal addressin cell adhesion molecule-1, J. Immunol. 156 (1996) 3727–3736.
[13] T. Schweighoffer, Y. Tanaka, M. Tidswell, D.J. Erle, K.J. Horgan, G.E.G. Luce, A.I. Lazarovits, D. Buck, S. Shaw, Selective expression of integrin $\alpha_4\beta_7$ on a subset of human CD4+ memory T cells with hallmarks of gut-trophism, J. Immunol. 151 (1993) 717–729.
[14] W.W. Agace, T-cell recruitment to the intestinal mucosae, Trends Immunol. 29 (2008) 514–522.
[15] S.I. Hammerschmidt, M. Ahrendt, U. Bode, B. Wahl, E. Kremmer, R. Forster, O. Pabst, Stromal mesenteric lymph node cells are essential for the generation of gut-homing T cells *in vivo*, J. Exp. Med. 205 (2008) 2400–2483.
[16] J. Arthos, C. Cicala, E. Martinelli, K. Macleod, D.V. Ryk, D. Wei, Z. Xiao, T.D. Veenstra, T.P. Conrad, R.A. Lempicki, S. McLaughlin, M. Pascuccio, R. Gopaul, J. McNally, C.C. Cruz, N. Censoplano, E. Chung, K.N. Reitano, S. Kottilil, D.J. Goode, A.S. Fauci, HIV-1 envelope protein binds to and signals through integrin $\alpha_4\beta_7$, the gut mucosal homing receptor for peripheral T cells, Nat. Immunol. 9 (2008) 301–309.
[17] S. Kewenig, T. Schneider, K. Hohloch, K. Lamps-Dreyer, R. Ullrich, N. Stolte, C. Stahl-Hennig, F.J. Kaup, A. Stallmach, M. Zeitz, Rapid mucosal CD4(+) T-cell depletion and enteropathy in simian immunodeficiency virus-infected rhesus macaques, Gastroenterology 116 (1999) 1115–1123.
[18] N.L. Letvin, N.W. King, Immunologic and pathologic manifestations of the infection of rhesus monkeys with simiam immunodeficiency virus of macaques, J. Acqui. Immune. Defic. Syndr. 3 (1990) 1023–1040.
[19] N. Onlamoon, K. Pattanapanyasat, A.A. Ansari, Human and nonhuman primate lentiviral infection and autoimmunity, Ann. NY Acad. Sci. 1050 (2005) 397–409.
[20] P.P. Firpo, I. Axberg, M. Scheibel, E.A. Clark, Macaque CD4+ T-cell subsets: influence of activation on infection by simian immunodeficiency viruses (SIV), AIDS Res. Hum. Retroviruses. 8 (1992) 357–366.
[21] A. Kaur, R.M. Grant, R.E. Means, H. McClure, M. Feinberg, R.P. Johnson, Diverse host responses and outcomes following simian immunodeficiency virus SIVmac239 infection in sooty mangabeys and rhesus macaques, J. Virol. 72 (1998) 9597–9611.
[22] M.R. Reynolds, E. Rakasz, P.J. Skinner, C. White, K. Abel, Z.M. Ma, L. Compton, G. Napoe, N. Wilson, C.J. Miller, A. Haase, D.I. Watkins, CD8+ T-lymphocyte response to major immunodominant epitopes after vaginal exposure to simian immunodeficiency virus: too late and too little, J. Virol. 79 (2005) 9228–9235.
[23] G. Silvestri, A. Fedanov, S. Germon, N. Kozyr, W.J. Kaiser, D.A. Garber, H. McClure, M.B. Feinberg, S.I. Staprans, Divergent host responses during primary simian immunodeficiency virus SIVsm infection of natural sooty mangabey and nonnatural rhesus macaque hosts, J. Virol. 79 (2005) 4043–4054.
[24] R.S. Veazey, I.C. Tham, K.G. Mansfield, M. DeMaria, A.E. Forand, D.E. Shvetz, L.V. Chalifoux, P.K. Sehgal, A.A. Lackner, Identifying the target cell in primary simian immunodeficiency virus (SIV) infection: highly activated memory CD4(+) T cells are rapidly eliminated in early SIV infection *in vivo*, J. Virol. 74 (2000) 57–64.
[25] A.A. Lackner, R.S. Veazey, Current concepts in AIDS pathogenesis: insights from the SIV-macaque model, Annu. Rev. Med. 58 (2007) 461–476.
[26] A.I. Lazarovits, R.A. Moscicki, J.T. Kurnik, D. Camerini, A.K. Bhan, L.G. Baird, M. Erikson, R.B. Colvin, Lymphocyte activation antigens: A monoclonal antibody, anti-Act1, defines a new late lymphocyte activation antigen, J. Immunol. 133 (1984) 1857–1862.
[27] M.J. Benson, K. Pino-Lagos, M. Rosemblatt, R.J. Noelle, All-trans retinoic acid mediates enhanced T reg cell growth, differentiation, and gut homing in the face of high levels of co-stimulation, J. Exp. Med. 204 (2007) 1765–1774.
[28] J.L. Coombes, K.R.R. Siddiqui, C.V. Arancibia-Carcamo, J. Hall, C.-M. Sun, Y. Belkaid, F. Powrie, A functionally specialized population of CD103+ DCs induces FoxP3+ regulatory T cells via a TGF-β- and retinoic acid-dependent mechanism, J. Exp. Med. 204 (2007) 1757–1764.
[29] M. Iwata, A. Hirakiyama, Y. Eshima, H. Kagechika, C. Kato, S.Y. Song, Retinoic acid imprints gut-homing specificity on T cells, Immunity 21 (2004) 458–466.
[30] B. Johansson-Lindbom, M. Svensson, O. Pabst, C. Palmqvist, G. Marquez, R. Förster, W.W. Agace, Functional specialization of gut CD103+ dendritic cells in the regulation of tissue-selective T cell homing, J. Exp. Med. 202 (2005) 1063–1073.
[31] S.G. Kang, H.W. Lim, O.M. Andrisani, H.E. Broxmeyer, C.H. Kim, Vitamin A metabolites induce gut-homing FoxP3+ regulatory T cells, J. Immunol. 179 (2007) 3724–3733.
[32] A.J. Stagg, M.A. Kamm, S.C. Knight, Intestinal dendritic cells increase T cell expression of alpha4beta7 integrin, Eur. J. Immunol. 32 (2002) 1445–1454.
[33] N.R. Klatt, F. Villinger, P. Bostik, S.N. Gordon, L. Pereira, J.D. Estes, J.C. Engram, A. Mayne, R.M. Dunham, B. Lawson, D.L. Sodora, S.I. Staprans, K. Reimann, G. Silvestri, A.A. Ansari, The availability of activated CD4+ T cells is a major determinant of set point viremia during natural SIV infection of sooty mangabeys, J. Clin. Invest. 118 (2008) 2039–2049.
[34] L.E. Pereira, R.P. Johnson, A.A. Ansari, Sooty mangabeys and rhesus macaques exhibit significant divergent natural killer cell responses during both acute and chronic phases of SIV infection, Cell Immunol. 254 (2008) 10–19.
[35] F. Villinger, G.T. Brice, A.E. Mayne, P. Bostik, K. Mori, C.H. June, A.A. Ansari, Adoptive transfer of simian immunodeficiency virus (SIV) naive autologous CD4+ cells to macaques chronically infected with SIV is sufficient to induce long-term nonprogressor status, Blood 99 (2002) 590–599.

[36] J.M. Bator, C.L. Reading, Measurement of antibody affinity for cell surface antigens using an enzyme linked immunosorbent assay, J. Immunol. Meth. 125 (1989) 167–176.
[37] M.A. Cromwell, R.S. Veazey, J.D. Altman, K.G. Mansfield, R. Glickman, T.M. Allen, D.I. Watkins, A.A. Lackner, R.P. Johnson, Induction of mucosal homing virus-specific CD8+ T lymphocytes by attenuated simian immunodeficiency virus, J. Virol. 74 (2000) 8762–8766.
[38] D.T. Evans, L.M. Chen, J. Gillis, K.C. Lin, B. Harty, G.P. Mazzara, R.O. Donis, K.G. Mansfield, J.D. Lifson, R.C. Desrosiers, J.E. Galan, R.P. Johnson, Mucosal priming of simian immunodeficiency virus-specific cytotoxic T-lymphocyte responses in rhesus macaques by the Salmonella type III secretion antigen delivery system, J. Virol. 77 (2003) 2400–2409.
[39] S.R. Reese, K.A. Kudsk, L. Genton, S. Ikeda, L-selectin and alpha4beta7 integrin, but not ICAM-1, regulate lymphocyte distribution in gut-associated lymphoid tissue of mice, Surgery 137 (2005) 209–215.
[40] M.A. Wurbel, M. Malissen, D. Guy-Grand, E. Meffre, M.C. Nussenzweig, M. Richelme, A. Carrier, B. Malissen, Mice lacking the CCR9 CC-chemokine receptor show a mild impairment of early T- and B-cell development and a reduction in T-cell receptor gammadelta(+) gut intraepithelial lymphocytes, Blood 98 (2001) 2626–2632.
[41] B.G. Feagan, G.R. Greenberg, G. Wild, R.N. Fedorak, P. Paré, J.W. McDonald, A. Cohen, A. Bitton, J. Baker, R. Dubé, S.B. Landau, M.K. Vandervoort, A. Parikh, Treatment of active Crohn's disease with MLN0002, a humanized antibody to the alpha4beta7 integrin, Clin. Gastroenterol. Hepatol. 6 (2008) 1370–1377.
[42] B.G. Feagan, G.R. Greenberg, G. Wild, R.N. Fedorak, P. Pare, J.W. McDonald, R. Dube, A. Cohen, A.H. Steinhart, S. Landau, R.A. Aguzzi, I.H. Fox, M.K. Vandervoort, Treatment of ulcerative colitis with a humanized antibody to the alpha4beta7 integrin, N. Engl. J. Med. 352 (2005) 2499–2507.
[43] T.K. Teaugue, A.I. Lazarovits, B.W. McIntyre, Integrin alpha4beta7 co-stimulation of human peripheral blood T cell proliferation, Cell Adhes. Commun. 2 (1994) 539–547.
[44] R.J.D. Boer, H. Mohri, D.D. Ho, A.S. Perelson, Turnover rates of B cells, T cells, and NK cells in simian immunodeficiency virus-infected and uninfected rhesus macaques, J. Immunol. 170 (2003) 2479–2487.
[45] H. Mohri, S. Bonhoeffer, S. Monard, A.S. Perelson, D.D. Ho, Rapid turnover of T lymphocytes in SIV-infected rhesus macaques, Science 279 (1998) 1223–1227.

Journal of Human Genetics (2009) 54, 224–229

www.nature.com/jhg

ORIGINAL ARTICLE

Complex divergence at a microsatellite marker *C1_2_5* in the lineage of *HLA-Cw/-B* haplotype

Daisuke Shichi[1], Masao Ota[2], Yoshihiko Katsuyama[3], Hidetoshi Inoko[4], Taeko K Naruse[1] and Akinori Kimura[1,5]

The human leukocyte antigen (HLA) complex locus has shaped a framework for evolutionary processes because of the dense clustering and strong linkage disequilibrium (LD) of polymorphic genes. Although the landscape of LD among conventional single-nucleotide polymorphisms (SNPs) has been described, the data on the lineage of major histocompatibility complex (MHC) haplotype are limited to pairwise comparisons of several haplotypes in Caucasoid populations. Multi-allelic markers, including microsatellite markers, may provide us with a larger power to analyze the MHC haplotype lineage because the mutation rate of microsatellite exceeds that of SNPs by several orders of magnitude. In this study, we investigated the complex structure of repeat motifs in a microsatellite to figure out the structural lineage of *HLA-Cw/-B* segments in Japanese. It was found that the genetic differences of *HLA-Cw/-B* haplotype lineage were reflected by repeat motif patterns at *C1_2_5* locus, suggesting that unique mutational dynamics of microsatellites may be a useful marker to chase the haplotype lineage.
Journal of Human Genetics (2009) **54,** 224–229; doi:10.1038/jhg.2009.15; published online 27 February 2009

Keywords: C1_2_5; HLA; microsatellite; repeat motif

INTRODUCTION

The human major histocompatibility complex (MHC), the human leukocyte antigen locus (HLA) on chromosome 6p21.3, spans about 4 Mb and contains many polymorphic genes relevant to the adaptive immune system.[1] Among them, genes for classical HLA molecules play pivotal roles in the immunological recognition of self versus non-self through presentation of antigenic peptides from either intracellular or extracellular origin.[2] Most of the extensive polymorphisms in the *HLA* genes were found at the peptide-binding groove of HLA molecules, thereby defining the bound peptides.[3] The HLA alleles at a given locus differ from each other by 1–30 amino acids at the protein level[4] and have been designated by the four-digit number or more according to the patterns of single-nucleotide polymorphisms (SNPs) and insertion–deletion polymorphisms within the coding sequence. The difference in allele distribution among different ethnic groups may be shaped by selective and demographic history.[5] It is well known that there is a strong linkage disequilibrium (LD) among alleles of genes in *HLA* locus, and combination of these alleles in LD form specific haplotypes.[6] Owing to the functional significance of classical *HLA* genes, the MHC haplotypes have been defined by using classical *HLA* alleles as highly polymorphic markers, and the *HLA* haplotypes served as a model system for high-resolution mapping of disease susceptibility genes,[7] evolution[8] and population structure.[9]

Detailed information on allelic diversity, recombination hotspot and profiles of LD within the MHC region are available,[6] but data on the lineage of the MHC haplotype and its evolution are not complete. The MHC Haplotype Sequencing Project was designed to elucidate the complete MHC genetic maps of several common Caucasian MHC haplotypes,[10] but little information is available for MHC haplotypes from different ethnic groups other than that from the Caucasians. Using selected genomic variation, including SNPs, individual MHC haplotypes can be characterized. This strategy has been used extensively to resolve the structure of the *HLA* allelic composition of SNPs and to determine new *HLA* alleles.[11] However, conventional SNP-based tagging could not adequately provide a resolution to capture the characteristics of variations of the MHC region at the worldwide population level. In other words, genetic markers other than SNPs, including copy number variations (CNVs) and microsatellites, might provide additional information in tracing the differentiation of the MHC haplotype.

Microsatellites, in general, undergo rapid change because of the insertion or deletion of one or multiple repeat units, primarily through replication slippage.[12] Moreover, the mutation rate of microsatellites (10^{-5}–10^{-3} per generation) exceeds that of SNPs and CNVs by several orders of magnitude. The difference in the mutational dynamics suggested that the microsatellites may be useful in tracing recent divergence in the structure of MHC haplotypes. More than

[1]Department of Molecular Pathogenesis, Medical Research Institute, Tokyo Medical and Dental University, Tokyo, Japan; [2]Department of Legal Medicine, Shinshu University School of Medicine, Matsumoto, Japan; [3]Department of Pharmacy, Shinshu University Hospital, Matsumoto, Japan; [4]Department of Molecular Life Science, Tokai University School of Medicine, Isehara, Japan and [5]Laboratory of Genome Diversity, School of Biomedical Science, Tokyo Medical and Dental University, Tokyo, Japan
Correspondence: Professor A Kimura, Department of Molecular Pathogenesis, Medical Research Institute, Tokyo Medical and Dental University, 1-5-45 Yushima, Bunkyo-ku, Tokyo 113-8510, Japan.
E-mail: akitis@mri.tmd.ac.jp
Received 17 November 2008; revised 3 February 2009; accepted 4 February 2009; published online 27 February 2009

1000 polymorphic microsatellite markers have been described within the *HLA* region.[13–16] The microsatellite markers showed considerable polymorphism and strong LD with particular alleles of classical *HLA* loci composing of well-defined extended *HLA* haplotypes.[17] The *HLA* haplotypes can be separated into several blocks, including a haplotype block containing the *HLA-Cw* and *-B* genes, just centromeric to the MHC class I region, which is known to be one of the highest polymorphic loci in the human genome.[18] In this study, we analyzed the microsatellite diversity surrounding the *HLA-Cw/-B* loci to investigate the haplotype lineages in a Japanese population.

MATERIALS AND METHODS

Study population and genotyping methods

The study population consisted of 261 Japanese individuals selected at random. All subjects gave informed consent and the study was approved by the Research Ethics Committee of Medical Research Institute, Tokyo Medical and Dental University and Tokai University School of Medicine. Complete genotyping was achieved for classical *HLA* genes and nine microsatellite markers from all individuals were enrolled in this study. Deviation from the Hardy–Weinberg equilibrium was tested for each *HLA* locus and each microsatellite marker. None of the selected markers showed significant ($P<0.05$) deviation from the Hardy–Weinberg equilibrium. High-resolution *HLA* genotyping (at four-digit allele resolution) was carried out with a sequence-based typing method at the class I genes (*HLA-A*, *-B* and *-Cw*) as recommended by the 13th International Histocompatibility Workshop protocols (http://www.ihwg.org/) and/or manufacturer's instructions (Forensic Analytical, Hayward, CA, USA). When an ambiguity in the genotype assignment was observed in the sequence trace data, genotype was predicted from the allele frequency and LD information in the Japanese.[19] DNA regions spanning the microsatellite polymorphisms were amplified by PCR using primer pairs under the conditions listed in Table 1, and the sequenced reference B-cell line samples, COX and PGX, were used as standard for sizing assignment of microsatellite.[20] In addition, to show the motif variation at *C1_2_5* locus, we sequenced the PCR products obtained from each subject on both strands. The number of repeat units was determined by the direct sequencing along with the fragment length analysis. A part (about 38%) of the subjects was also investigated for the *C1_2_5* allele by cloning the PCR products using the TA cloning kit (Invitrogen, Carlsbad, CA, USA). Data from the cloning of *C1_2_5* were completely consistent with the genotyping data obtained from the direct sequencing method.

Phylogenetic analysis

Sequence data on the *HLA-Cw* alleles (exon 4) were obtained from the IMGT/HLA sequence database (http://www.ebi.ac.uk/imgt/hla/index.html). Sequence alignments of the alleles were created by using GENETYX version 8.1.2 (GENETYX CORPORATION, Tokyo, Japan). Phylogenetic analyses were performed using the unweighted pair group method using arithmetic average (UPGMA) by the MEGA software Version 4.0 (http://www.megasoftware.net/).

Statistical analysis

Deviation from the Hardy–Weinberg equilibrium was tested for all marker loci by using the PyPop v.0.6.0 software package (http://www.pypop.org/).[21] The expectation–maximization algorithm implemented in the 'haplo_stat' package for R statistics software (http://www.r-project.org/)[22] was used to construct haplotypes and estimate their frequencies. The strength of pairwise LD between the alleles of classical *HLA* genes and/or microsatellite markers was quantified by two LD coefficients, D' and r^2, through the add-on R software package 'genetics'.[23] We also evaluated the associations between the *HLA-B* and *HLA-Cw* alleles by sensitivity and specificity; sensitivity was defined as the probability of observing the *HLA-B* allele when a particular *HLA-Cw* allele was observed, whereas specificity was the probability of not observing the *HLA-B* allele in the absence of the particular *HLA-Cw* allele. The long-range association was investigated by the extended haplotype homozygosity (EHH) statistic that was calculated according to the formula developed by Sabeti *et al.*[24] Overall LDs between two loci were estimated by using two statistics, Hedrick's multi-allelic D'[25] and Cramer's V.[26] When there are only two alleles per locus, Cramer's V is equivalent to the correlation coefficient between the two loci. Statistical significance of the LD between pairs of loci was tested using a permutation test with 1000 permutations for each locus pair.

RESULTS

Association between *HLA-B* and *-Cw* gene loci

Significant associations between the alleles of *HLA-Cw* and *HLA-B* genes were found among 261 Japanese individuals as expected from the physical proximity of *HLA-Cw* and *-B* (85 kb). Of the 75 different

Table 1 Primer sets for microsatellite genotyping around the *HLA-B/-Cw* loci

Marker name	*Position*[a]	*Repeat unit*	*PCR product size [bp]*	*Primer sequence (5′–3′)*	*Dye*	*PCR condition*[b]
C2_4_4	31697425–31697663	(GAAA)	181–281	GGCTTGACTTGAAACTCAGAGACC	Hex	i
				TTATCTACTTATAGTCTATCACGG	—	
C1_3_1	31884120–31884408	(TTG)	279–345	CAGTGACAAGCACCTGGCAC	Tet	i
				GCCAGATGTGGTGGCATGC	—	
C1_2_5	31367081–31367280	(CA)	178–220	CAGTAGTAAGCCAGAAGCTATTAC	6-Fam	i
				AAGTCAAGCATATCTGCCATTTGG	—	
C1_4_1	31439129–31439353	(AAAC)	171–271	CGAGAGAACAACTGGCAGGACTG	6-Fam	i
				GACAGTCCTCATTAGCGCTGAGG	—	
MIB	31457335–31457670	(CA)	326–356	CTACCATGACCCCCTTCCCC	Hex	i
				CCACAGTCTCTATCAGTCCA	—	
STR_MICA	31488069–31488251	(GCT)	179–194	CCTTTTTTTCAGGGAAAGTGC	6-Fam	i
				CCTTACCATCTCCAGAAACTGC	—	
C1_2_A	31579685–31579926	(CA)	234–264	AATAGCCATGAGAAGCTATGTGGGGGAG	6-Fam	ii
				CTACCTCCTTGCCAAACTTGCTGTTTGTG	—	
TNFa	31643387–31643503	(AC)	61–161	CCTCTCTCCCCTGCAACACACA	6-Fam	i
				GCCTCTAGATTTCATCCAGCCACA	—	
TNFd	31664102–31664231	(TC)	131–137	AGATCCTTCCCTGTGAGTTCTGCT	Hex	i
				CATAGTGGGACTCTGTCTCCAAAG	—	

[a]The chromosome 6 genomic sequences was used as a reference.
[b]The PCR was carried out in an ABI9700 thermal cycler under the following conditions: (i) 12 min at 95 °C followed by 35 cycles of 95 °C for 30 s, 55 °C for 45 s, 72 °C for 1 min and final extension for 10 min at 72 °C; (ii) 2 min at 94 °C followed by 30 cycles of 94 °C for 1 min, 55 °C for 1 min, 72 °C for 2 min, with an additional 5 min final extension at 72 °C.

Table 2 Association performance of *HLA-Cw/-B* haplotypes in a Japanese population

HLA-B/-Cw haplotype	*Haplotype frequency*	*D'*	*Hill's r^2*	*Sensitivity[a] (%)*	*Specificity[b] (%)*
*Cw*1202-B*5201*	0.144	0.98	0.93	97.4	98.9
*Cw*0102-B*5401*	0.092	0.94	0.32	94.1	84.9
*Cw*0303-B*1501*	0.036	0.40	0.12	45.2	92.3
*Cw*0304-B*4002*	0.054	0.77	0.34	77.8	93.4
*Cw*0102-B*4601*	0.057	0.91	0.19	90.9	81.8
*Cw*0702-B*0702*	0.061	0.96	0.43	97.0	93.0
*Cw*0303-B*3501*	0.042	0.66	0.24	68.8	93.1
*Cw*0304-B*4001*	0.034	0.53	0.14	58.1	91.4
*Cw*1403-B*4403*	0.057	1.00	0.93	96.8	99.8
*Cw*1402-B*5101*	0.048	0.06	0.76	80.6	99.8

[a]Sensitivity: the probability of observing the particular *HLA-Cw* allele given the presence of the particular *HLA-B* allele.
[b]Specificity: the probability of not observing the particular *HLA-Cw* allele given the absence of the particular *HLA-B* allele.

HLA-B and *-Cw* allele combinations observed, 10 were relatively common with haplotype frequency above 3%, by which 63% of the Japanese panels could be explained (Table 2). Two combinations, *Cw*1202-B*5201* and *Cw*1403-B*4403*, showed high correlations (over 0.90) for sensitivity, specificity, D' and r^2. In contrast, *HLA-Cw/-B* haplotypes containing *Cw*0102*, *Cw*0303* and *Cw*0304* showed less association, although these haplotypes could account for a considerable part in the Japanese population, because these *HLA-Cw* alleles composed of several haplotypes with different *HLA-B* alleles.

Long-range haplotype around the *HLA-B* and *-Cw* genes

To analyze a long-range structure of the region, EHH analysis was performed, which enabled us to estimate the length of LD from the alleles of a landmark locus. As illustrated in Figure 1, each EHH profile within the 300 kb from the landmark tended to decline the LD with increasing distance from the landmark as expected. However, the pattern of EHH varied substantially, depending on the allele at the landmark locus and on the two-locus haplotype. The haplotypes landmarked by the alleles of *HLA-Cw* and *-B* genes extended longer to telomeric side (MHC class I region) and centromeric side (MHC class II region), respectively (Figures 1a–d). Nevertheless, *HLA-Cw/-B* haplotypic combinations (for example, *Cw*1202* and *B*5201*, *Cw*1403* and *B*4403*) formed by almost one-to-one correspondence showed the long-range LD. In clear contrast, others (for example, *Cw*0102*, *Cw *0303* and *Cw *0304*) with highly diverged combinations rapidly diminished the EHH score even within approximately 100 kb around the landmark locus (Figure 1b). As a rapid EHH decay was found at the *C1_2_5* locus around 22.1 kb centromeric to the *HLA-Cw* locus, we examined the EHH pattern from the landmark of two-locus haplotype extended from *C1_2_5* to either *HLA-B* or *-Cw* locus. The degree of EHH decay from the haplotypes of *HLA-B* or *-Cw* coupled with *C1_2_5* showed a similar tendency to that obtained from the landmark of *HLA-B* or *-Cw* alone. Interestingly, it was found that the EHH pattern was different between *Cw*0702* and *Cw*0303* even though these two *HLA-Cw* alleles were linked to the identical allele, *C1_2_5*200* (Figure 1d). As expected, the EHH scores of *HLA-Cw/-B* haplotypes tended to maintain a long-range LD extending centromeric and teromeric to the landmark locus (Figure 1e). These observations suggested that the diversity of *C1_2_5* locus at the nucleotide level was well correlated with the lineage of the *HLA-Cw/-B* haplotype.

Structural analysis of *C1_2_5* marker

To further delineate the haplotypic structure of the *HLA-Cw/-B* region, we focused on the motif structure of a microsatellite marker, *C1_2_5*, which was located between *HLA-B* and *HLA-Cw*. Sequencing analysis of *C1_2_5* revealed four motifs consisting of nucleotide substitutions in addition to gain or loss of CA repeat units (Figure 2a). These substitutions *per se* were observed within the repeat tract and hence did not change the size of PCR fragments, whereas the differences of the motif structure provided us with the additional information on diversity, as exemplified by *C1_2_5*200* and *C1_2_5*218*. Using these data, genetic associations between *C1_2_5* alleles and individual *HLA-Cw/-B* alleles were investigated to characterize the diversity of HLA haplotypes. The $(CA)_nCTCA$ and $(CA)_4AA(CA)_5AA(CA)_nCTCA$ motifs were in tight LD with *Cw*0801* and *Cw*0102*, respectively, and the majority of *C1_2_5* alleles showed strong LD, with particularly *HLA-Cw* alleles, but there were several exceptions. For example, *Cw*0304* was in LD with three different *C1_2_5* variations, $(CA)_4AA(CA)_{19}CTCA$, $(CA)_4AA(CA)_{21}CTCA$ and $(CA)_4AA(CA)_{23}TACACTCA$. The former two variations forming the identical *HLA-Cw/-B* haplotype, *Cw*0304-B*4002*, should be derived from the same repeat motif. In contrast, the third variation with different motif was linked to a different HLA-B allele, *B*4001*, forming the *Cw*0304-B*4001* haplotype.

Phylogenetic relationship between alleles of *C1_2_5* and *HLA-Cw*

The mutation rate of SNP was estimated to be 10^{-8} per generation, whereas that of microsatellite was between 10^{-5} and 10^{-3} per generation.[27] Relationships among *C1_2_5* alleles with four motifs were phylogenetically analyzed (Figure 2a). Of four major motifs, the simplest structure was $(CA)_nCTCA$, observed in short alleles of both *C1_2_5*188* and **192*. All other *C1_2_5* alleles had a (CA) to (AA) change at the fifth CA unit, resulting in a motif sequences $(CA)_4AA(CA)_n$, interrupting the CA repeat array. In addition, *C1_2_5* alleles containing the interrupting sequence, $(CA)_4AA(CA)_n$, can be subdivided into two different motifs as follows; $(CA)_4AA(CA)_nTACACTCA$ resulted from a (CA) to (TA) change in 3'-side of the CA repeat and $(CA)_4AA(CA)_5AA(CA)_nCTCA$ resulted from CA-to-AA change at the 11th unit. As all microsatellite motifs shared the simplest motif, it was assumed that $(CA)_nCTCA$ was the core structure of the *C1_2_5* microsatellite. On the other hand, to investigate the relationships of lineage between the *C1_2_5* motif structures and the neighboring SNPs, we constructed a phylogenetic tree using the exon 4 sequences of *HLA-Cw* alleles, which encoded the α3 domain, to exclude the effects of selective pressure acting on the peptide-binding domain (Figure 2b). It was found that the relationship among *C1_2_5* alleles (microsatellite lineage) was not always concordant with the relationship of *HLA-Cw* alleles (SNPs lineage).

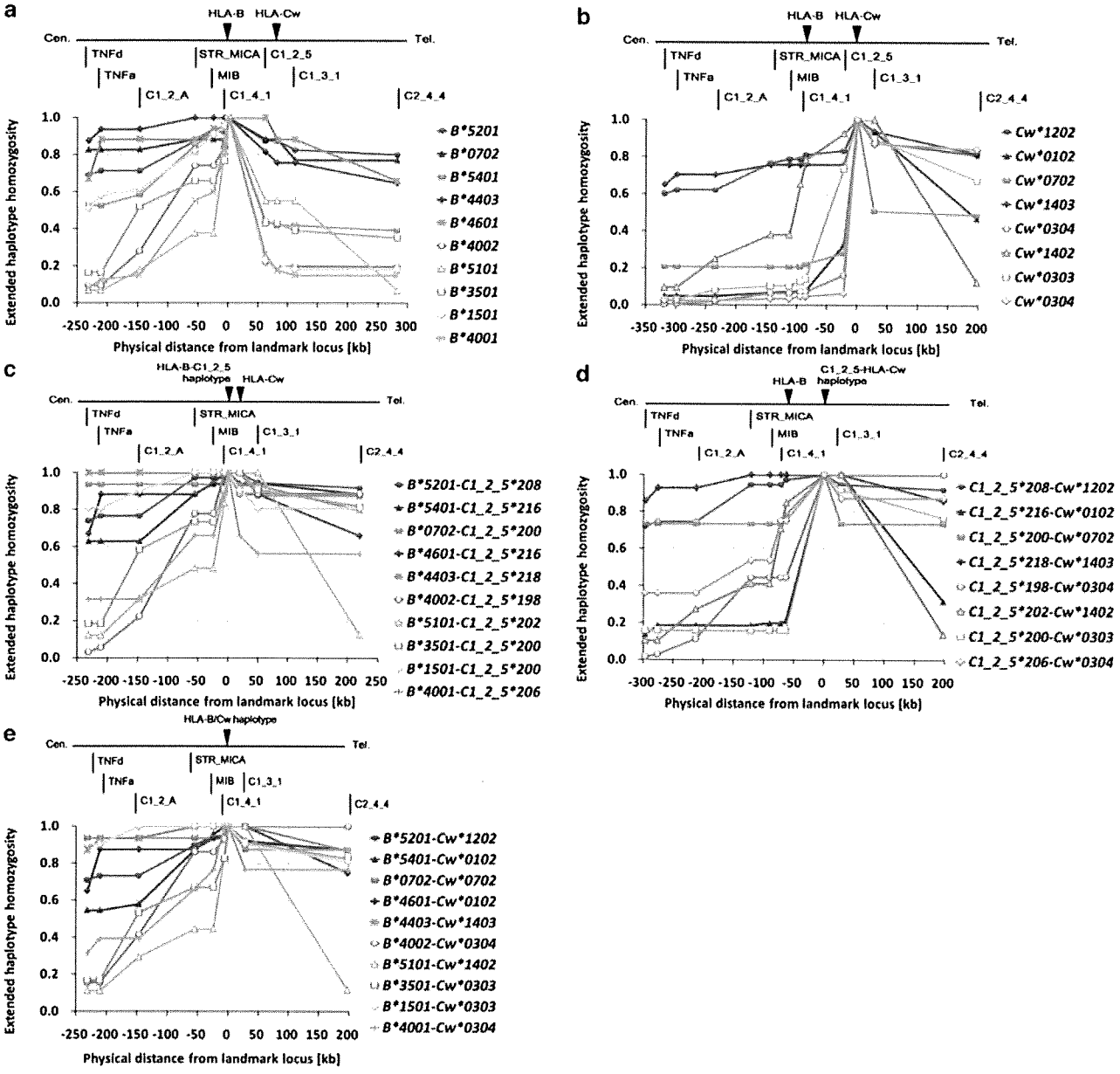

Figure 1 Long-range haplotype test using classical *HLA* genes and microsatellite markers. Each plot represents the extended haplotype homozygosity (EHH) values spanning about 200–300 kb from alleles at two landmark loci, (**a**) *HLA-B* and (**b**) *HLA-Cw*, and three two-locus haplotypes, (**c**) *HLA-B-C_1_2_5*, (**d**) *C1_2_5-HLA-Cw* and (**e**) *HLA-B-HLA-Cw*, in both directions. Vertical lines and arrowheads over the map indicate the locations of microsatellite markers and *HLA* loci, respectively. The gene map was obtained from the Wellcome Trust Sanger Institute (http://www.sanger.ac.uk/HGP/Chr6/MHC.shtml). The physical distances are given in kb, with negative and positive numbers used for locations proximal to and distal from the landmark, respectively.

Multiallelic analysis of LD between *C1_2_5* and its franking *HLA* genes

As the EHH analysis was focused on the LD among specific pairs of alleles and haplotypes with relatively high frequency (>3%), we also evaluated overall LDs between two loci among *HLA-B*, *-Cw* and *C1_2_5* to figure out the overall nature of the LD structure in this region (Table 3). It was found that the *C1_2_5* locus, at both the allele level and the motif level, showed stronger LD with *HLA-Cw/-B* haplotype than with either *HLA-B* or *-Cw* locus. These observations suggested that the divergence of *C1_2_5* locus reflected its tight association with the *HLA-Cw/-B* haplotype rather than the association with *HLA-Cw* alleles or *HLA-B* alleles.

DISCUSSION

In this study, we investigated whether a microsatellite marker adjacent to the most polymorphic *HLA-Cw/-B* loci could provide us with information to delineate the haplotype lineage. We found that the *C1_2_5* microsatellite was highly variable by three substitutions within the CA repeat array in addition to the number of CA repeats. The unique polymorphic patterns at *C1_2_5* locus were well correlated with the *HLA-Cw/-B* haplotypes. It was also shown that the simple analysis of fragment-size variation should overlook the nature of microsatellite variations.

The structure of repeat motif was attractive from the evolutional viewpoint because the microsatellite and *HLA-Cw* alleles appeared to